Effect of Radial Transport on Compressor Tip Clearance Flow Structures and Enhancement of Stable Flow Range
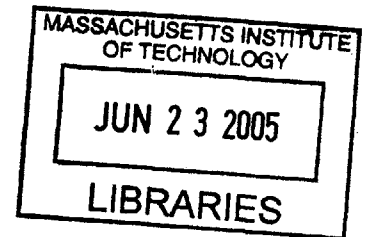
by

Sean Nolan

B.S, Aeronautics and Astronautics, Massachusetts Institute of Technology, 2003

Submitted to the Department of Aeronautics and Astronautics
in partial fulfillment of the requirements for the degree of

Master of Science in Aeronautics and Astronautics
at the
Massachusetts Institute of Technology

June 2005

Author: _____ _____
Department of Aeronautics and Astronautics
May 20, 2005

Certified by:____ _____
Edward M. Greitzer
H. N. Slater Professor of Aeronautics and Astronautics
Thesis Supervisor

Certified by:_____ _____
Douglas C. Rabe
AFRL Turbine Engine Research Center Director
Thesis Supervisor

Certified by:__ _____
Choon S. Tan
Senior Research Engineer
Thesis Supervisor

Accepted by:_____
Jaime Peraire
Professor of Aeronautics and Astronautics
Chair, Committee on Graduate Students

AERO

Effect of Radial Transport on Compressor Tip Flow Structures and Enhancement of Stable Flow Range

by

Sean Nolan

Submitted to the Department of Aeronautics and Astronautics on May 20, 2005 in partial fulfillment of the requirement for the Degree of Master of Science

Abstract

The relation between tip clearance flow structure and axial compressor stall is interrogated via numerical simulations, to determine how casing treatment can result in improved flow range. Both geometry changes and flow field body forces are used as diagnostics to assess the hypothesis that the radial transport of momentum out of the tip region, and the consequent decrease in streamwise momentum in this region, is a key aspect of the flow. The radial velocity responsible for this transport is a result of the flow field set up by the tip clearance vortex. Altering the position of the tip clearance vortex can alter the amount of streamwise momentum lost due to radial transport and hence increase the compressor flow range.

Circumferential grooves improve the flow range in the manner described above. In the presence of such a groove the radial velocity profile along the passage can be altered so that that the radial transport of streamwise momentum is decreased. The flow fields associated with grooves at different axial positions, and of different depths, are also examined, along with previous research on circumferential grooves, and it is shown that these are in accord with the hypothesis.

Thesis Supervisor: Edward M. Greitzer
Title: H. N. Slater Professor of Aeronautics and Astronautics

Thesis Supervisor: Douglas C. Rabe
Title: AFRL Turbine Engine Research Center Director

Thesis Supervisor: Choon S. Tan
Title: Senior Research Engineer

Acknowledgements

There are myriad persons I must thank for providing support and guidance in this research. My advisors, Professor E. M. Greitzer and Dr. Choon Tan, have been a great source of technical information regarding thermodynamics and fluid mechanics. More importantly, they have taught me much about the essence of technical research, an activity that is as much an art as it is a science.

Also providing invaluable advice was Dr. Douglas Rabe of the Compressor Research Facility at the Air Force Research Lab. My time working for him at the AFRL gave me much needed experience. There were several other people at AFRL who helped my research progress. They include David Car, Tom McCray, and Carl Williams. Dr. Chunill Hah of NASA Glenn also deserves thanks for his sharing of CFD knowledge and results.

At GTL, Dr. Yifang Gong and Dr. Boris Sirakov helped to greatly ease the learning curve associated with numerical simulation. For their work in providing an environment in which research can be done, Paul Warren, Lori Martinez, Julia Finn, and Holly Anderson also deserve a great deal of recognition.

I am indebted to the students of GTL, with whom ideas were discussed and refined. Parthiv Shah was especially important in this aspect. Apart from the technical help, my fellow students helped to make the atmosphere around the lab enjoyable.

I am grateful towards my roommates Michael Razo, Leilani Roser, and Andrew Wong. Many thanks also to Professor J.P. Clarke, Ben Schmeckpeper, Yuval Mazor, Brian Anderson, and the rest of the MIT track and field and cross country teams.

Most importantly, I want to thank my brother and my mom. My mom, Janice M. Rock-Nolan, has always provided advice and support, and the last two years were no exception.

Disclaimer

Table of Contents

List of Figures

7

List of Tables

Nomenclature

Symbols

ρ	density
q	dynamic head
A_b	blockage area
A	area
P	pressure
P_t	stagnation pressure
T	temperature
T_t	stagnation temperature
η	adiabatic efficiency
r	radial position
τ	tip clearance gap
U_t	blade tip speed
V'	Relative Velocity
u	velocity
μ	viscosity
$y+$	non-dimensional distance from wall
γ	specific heat ratio
ζ	angle between clearance flow and bulk flow
ϕ	flow coefficient

Subscripts

100	refers to 100%span (the radial plane level with the blade tip)
bp100	refers to the 100%span region within the blade passage
x	axial direction
θ	tangential direction
s	streamwise direction
r	radial direction
e	edge of velocity defect

Chapter 1

Introduction and Background

1.1 Compressor Performance and Use of Casing Treatment

The flow range in which an axial compressor can operate is an important

limitation in the operation of a gas turbine. As depicted in Fig. 1.1, if the mass flow

becomes too low for a given engine speed, compressor stall or surge will occur. The

result of the stall is either rotating stall or surge, two unsteady phenomena which can

have serious operational or mechanical consequences [Kerrebrock, 12]. Avoiding tall is

thus an important aspect of compressor design and development.
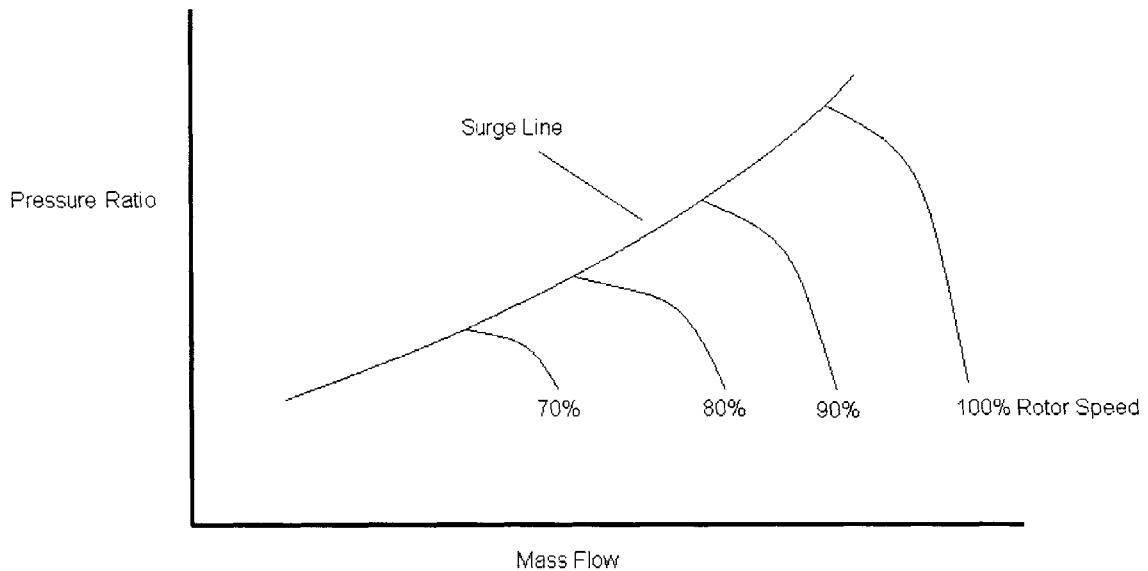
Figure 1.1 Sample compressor map

While stall can be initiated on the blade or in the tip region, for compressors with

moderate to high solidities, stall is initiated in the tip region [Koch, 14]. As depicted in

figure 1.2 [6], increased tip clearances result in decreased flow range, pressure rise, and

efficiency.
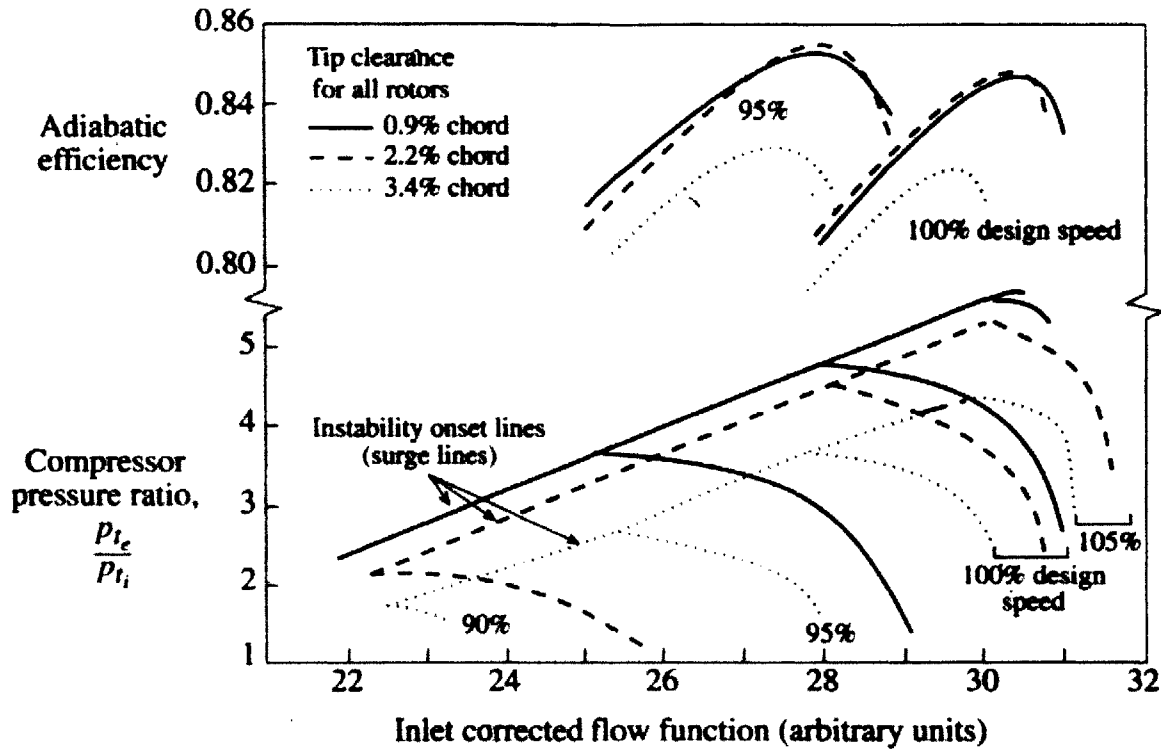
Figure 1.2 Effect of tip clearance on compressor performance. [Cumpsty, 6]

The buffer between the operating line and the stall line is called the stall margin. In spite of the design stall margin, the compressor may approach the stall line during transient operation or if the compressor is deteriorated due to increased tip clearance. If it is determined that stall margin is not adequate, often casing treatment has been incorporated to increase the useful flow range. Casing treatment consists of slots or grooves integrated into the casing above the blade tip (Figure 1.3, which is for a small helicopter engine).

The marked effect that tip casing treatments have indicates the significance of the tip region flow in setting the compressor stall limit. However, much of the knowledge regarding casing treatments and their effectiveness is empirical. Also, the flow range extension obtained through the use of casing treatment is often accompanied by a penalty in pressure rise coefficient and/or efficiency at the design condition (Figure 4). This

13

thesis addresses the mechanism of compressor stall and flow range enhancement by one type of casing treatment.

Figure 1.3 Sample casing treatment Figure [The Rolls-Royce Magazine]
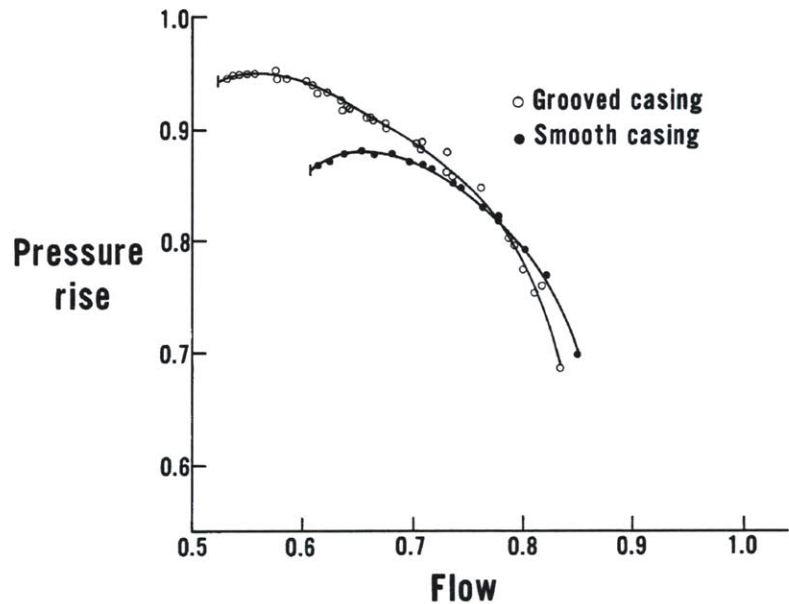
1.4 Typical effect of casing treatment [Greitzer, et al., 8]

1.2 Research Goals

The objective of this research is to be able to determine the changes in the flow field by which casing treatments improve compressor performance. This would in turn enable a design guideline for casing treatments to be developed. In order to do so, the following specific research questions must be answered:

- What are the critical aspects of tip flow that impact flow range?

- What are the changes that enhance flow range?

- What are the mechanisms of casing treatment which create these flow field changes?

1.3 Specific Research Contributions

- This research identifies a key flow feature (the radial velocity associated with the tip clearance vortex) that results in streamwise momentum being transported radially out of the tip region. Improvement of the radial transport term is shown to improve streamwise momentum at the blade tip and hence improve compressor flow range.

- Demonstration that circumferential groove casing treatments are shown to improve performance by improving radial transport and hence the loss of streamwise momentum in the blade tip region.

- Demonstration that for peak efficiency of circumferential groove treatment, there is an optimum depth, smaller than the tip clearance. If flow range is the sole concern, deeper grooves are better.

- Demonstration that circumferential grooves should be placed so that the tip clearance vortex is roughly parallel to the trailing edge of the groove.

- In-depth discussion of the cause and effect relationship between the use of casing treatment and improvement in flow range. The improvement is linked to repositioning of the tip clearance vortex further towards the trailing edge of the blade passage.

- A unified description including this research and previous research concerning tip clearance flow is presented relating blockage, backflow, streamwise momentum, and the tip clearance vortex.

Chapter 2 Previous Research and Hypothesis

2.1 Previous Research

Much research has been done to show the relation between tip clearance flows and the onset of compressor stall. Key results from previous research relevant to this work are described here.

Lee performed experiments on a stator row with a rotating hub [11]. Both smooth hubs and hubs with casing treatments were examined. It was shown that increasing the streamwise momentum (momentum in the blade-fixed frame projected onto the chordline of the blade) in the tip region resulted in improved performance, most notably the pressure rise at which the blade row stalled. The streamwise momentum increase was achieved through use of the casing treatment with axially skewed slots as well as through suction and blowing.

Crook[5] also found that increased streamwise momentum in the tip clearance improved flow range based on numerical simulations.

Khalid [13] developed a simple analysis for the relationship between tip clearance, loading, and blockage, defined as the momentum deficit calculated on a plane normal to the flow. Stall is closely related to blockage, in that the slope the curve of blockage vs. flow coefficient increases markedly as stall is approached. The definition for blockage proposed by Khalid is given in equation 1.

$$A_b = \iint 1 - \frac{\rho u}{\rho_e u_e} dA. \qquad (1)$$

In equation 1, the subscript "e" refers to the values at the edge of the momentum defect. region Flow blockage determines the pressure rise possible across the compressor, since

blockage reduces the effective flow area. Khalid found that the primary contributor to blockage is the expansion of the low relative total pressure region in the vortex core. Two key factors that determine blockage generation are thus the pressure rise through the blade passage and the magnitude of the relative total pressure deficit.

Fig. 2.1 shows the relation between nondimensional blockage and loading, computed by Khalid. On the y-axis, A_b represents the absolute blockage, while τ represents the tip clearance. On the x-axis, ΔP_t represents the change in relative total pressure experienced from upstream of the blade passage to the tip clearance vortex core, ΔP is the static pressure rise through the blade passage, and Q is the dynamic head a the inlet. Given a constant static pressure rise and dynamic head, as the total pressure defect in the vortex core becomes more pronounced, the blockage increases.
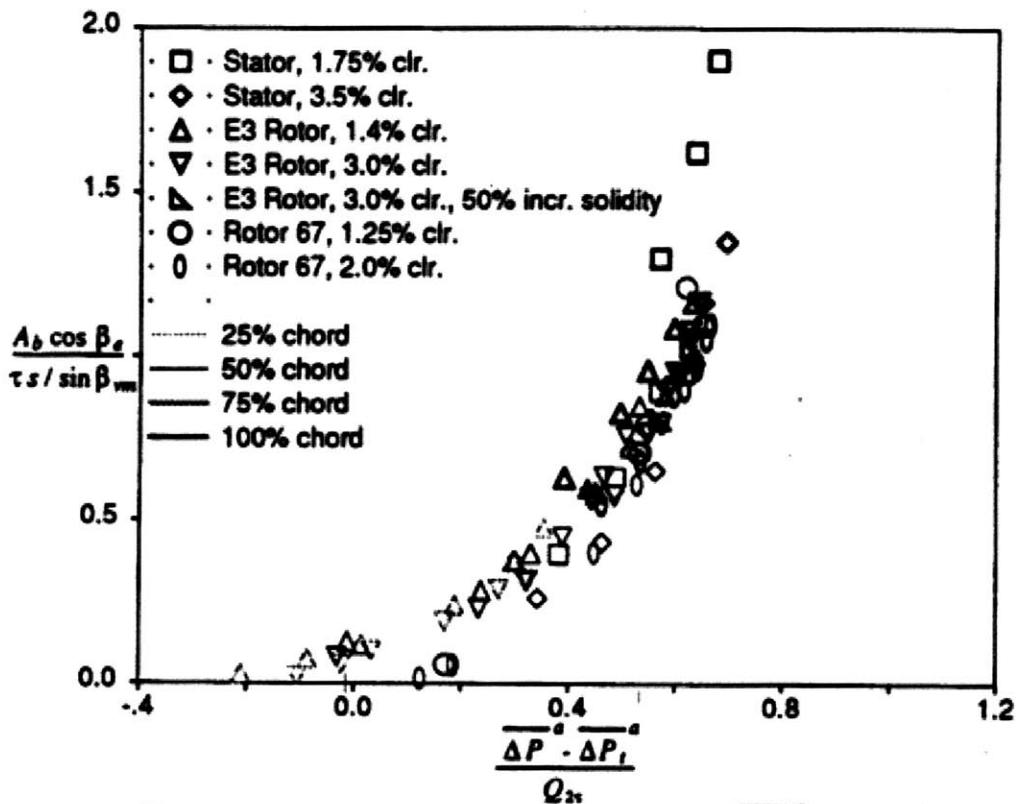
Figure 2.1 Non-Dimensional blockage vs. loading factor[Khalid, 13]

Rabe and Hah [15] studied the effect of a circumferential groove casing on a transonic rotor blade. It was determined that the stall point coincided with a particular incidence angle at the blade tip leading edge. The use of casing treatment lowers the overall flow coefficient at which this incidence angle was achieved, delaying stall. The stalling incidence angle, however, was found to be common between baseline and casing treatment cases, as shown in Fig. 2.2.

88.5°	84.8°	85.2°
Smooth wall (A)	Deep grooves (B)	Shallow grooves (C)

Flow incidence angles near pressure side at leading edge at smooth-wall stall mass flow rate.

90°	90°	90°
Deep grooves (D)	Shallow grooves (E)	Two shallow grooves (F)

Flow incidence angles near pressure side at leading edge at individual stall mass flow rates.
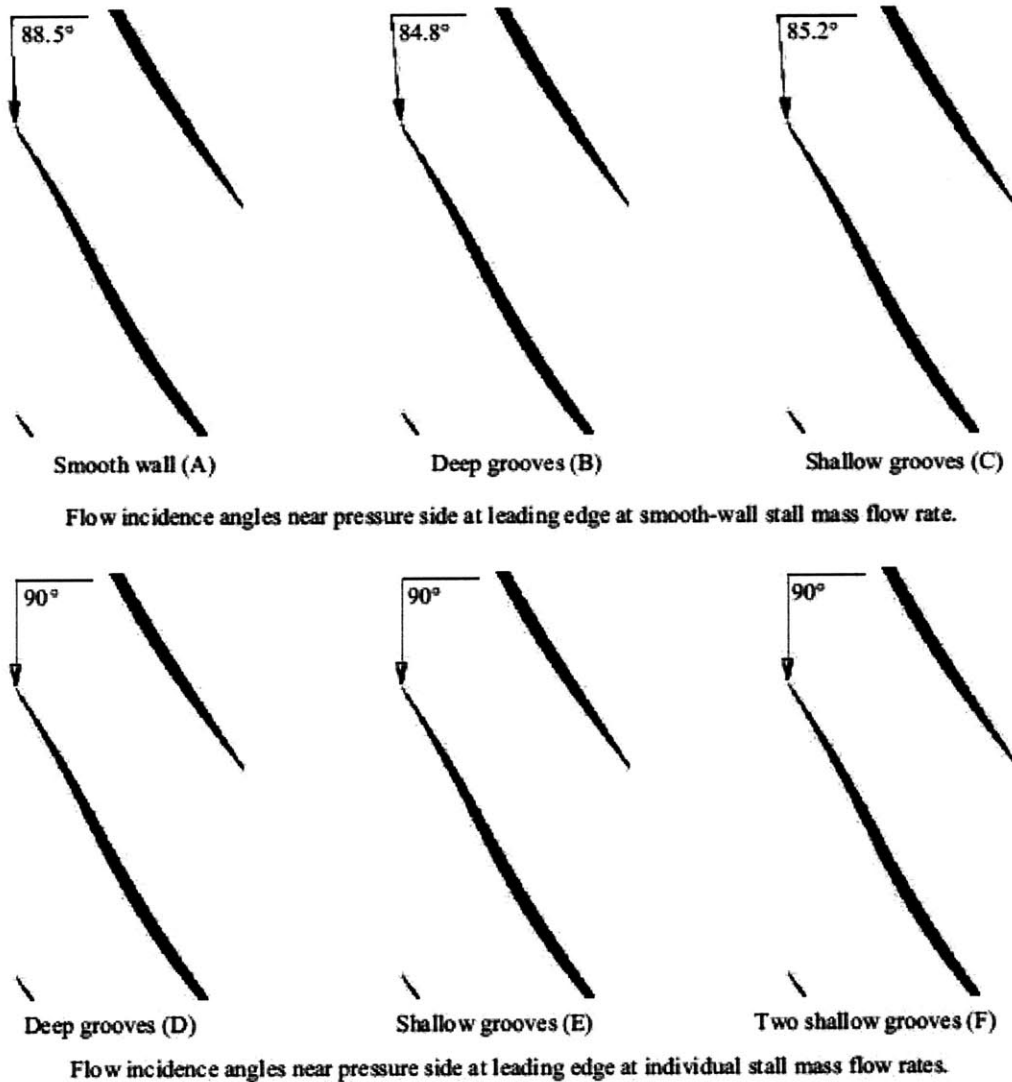
Figure 2.2 Incidence angle stall criterion. Casing treatment lowered the flow coefficient at which the critical incidence angle was reached [Rabe, 15]

It has been found that there are two routes to compressor rotating stall. Spike stall inception develops from a relatively short wavelengthed disturbance of 2-3 blade pitches. In contrast, modal inception occurs from low amplitude, long wavelength disturbances that take longer to develop into full stall [Camp, 3]. More details concerning the different paths of stall inception can be found in Appendix B. Vo [19] concluded that there are two flow features that are necessary and sufficient for spike stall onset to occur. There must be flow into the adjacent passage from around the trailing edge, and from around the leading edge (see figure 2.3) for spike stall to occur. The order in which these phenomena occur depends on the particular compressor configuration, but once they both occur spike stall will occur.
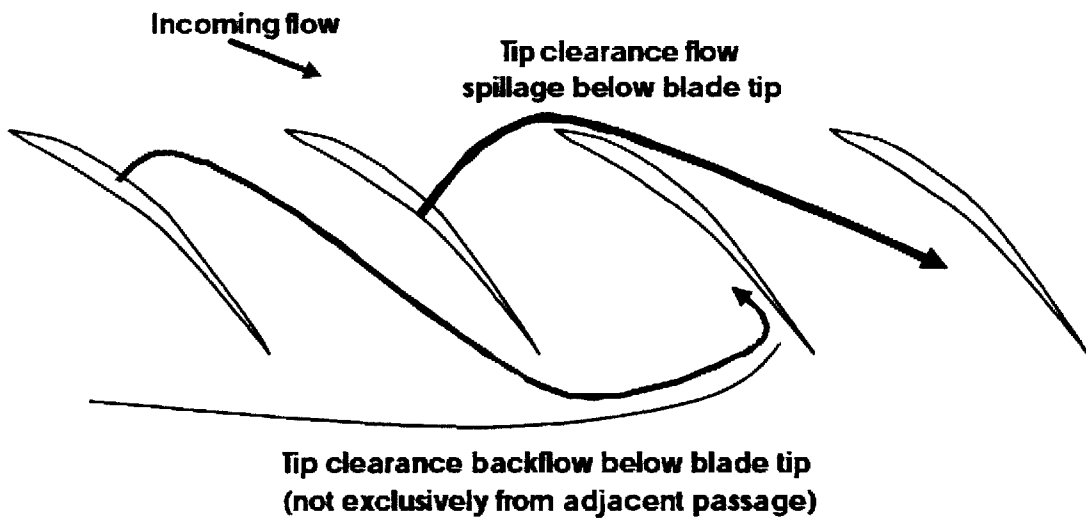
Figure 2. 3 Stall criteria of Vo[19]. Flow into the adjacent blade passage around the leading and trailing edges of the blade.

The tip clearance flow also has a large effect on efficiency. Storer and Cumpsty [17], used a control volume approach to show that the loss caused by mixing of the clearance flow with the mainstream flow increases as the angle, ζ , between clearance

19

and mainstream flows increases. Figure 2.4 shows if the clearance flow's streamwise momentum is increased, the angle will decrease, providing a possibility for loss reduction.
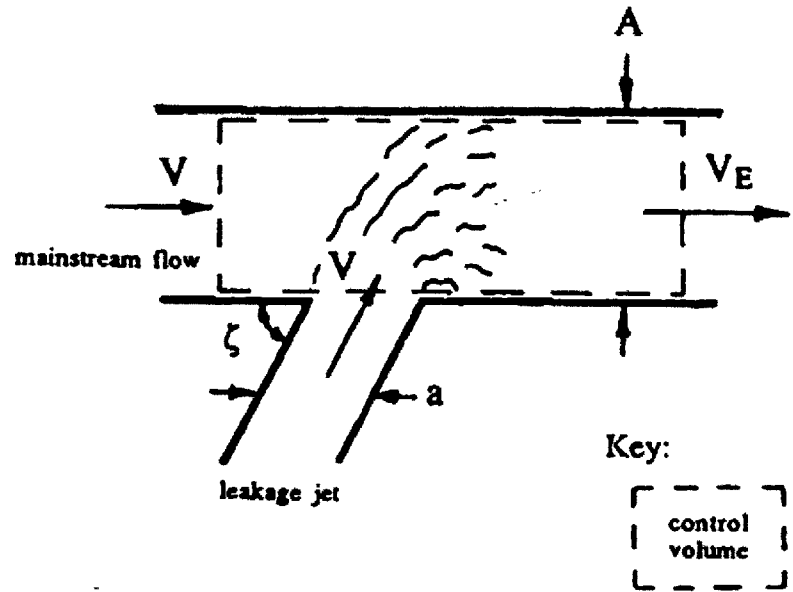
Model for predicting losses due to mixing between clearance and mainstream flows [Storer and Cumpsty, 17]
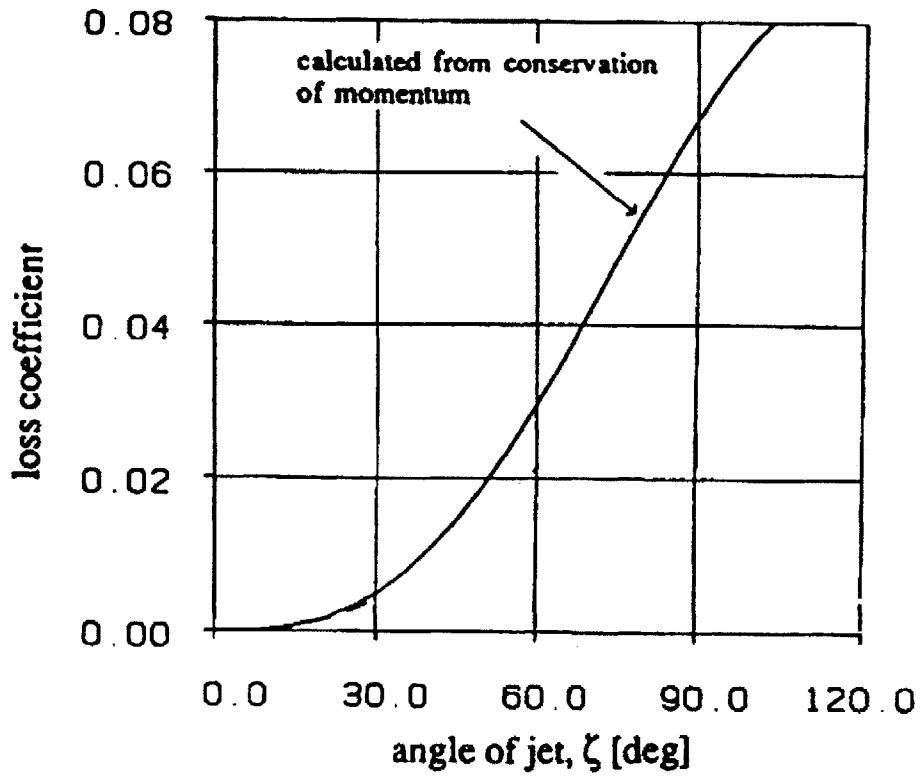
Figure 2.4 Losses due to mixing between clearance flow and bulk flow [Storer and Cumpsty, 17]

20

The previous research indicates that increased streamwise momentum at the blade tip can improve performance. Another question is how the measure of streamwise momentum relates to the blockage view and to the stall criteria identified by Vo [19] and Rabe and Hah [15]. The connection lies in the location from which the tip clearance fluid is drawn. The clearance flow can come from upstream or from the adjacent blade passage. Ideally, as much of the tip clearance flow as possible should come from upstream of the blade passage, since that is where the relative total pressure is greatest. Even near the design point, however, some fluid that goes into making the tip clearance vortex comes from an adjacent blade passage, and as a result has a total relative pressure deficit before entering the blade clearance. The formation of the clearance vortex further reduces the low total pressure.

As the streamwise momentum decreases, the proportion of reingested fluid increases, and the core of the clearance vortex experiences a severe drop in the relative total pressure. Figure 2.5 shows qualitatively how the source for the core of the clearance vortex changes as the compressor is throttled towards stall. As per Khalid's blockage relationship, this results in greater blockage, and hence a tendency to stall. The stall indicators highlighted by Vo and Rabe and Hah are qualitative measures of the streamwise momentum in certain regions near the tip. A high incidence angle at the leading edge, or backflow around the leading and trailing edges of the blades both indicate the streamwise momentum near the blade tip is low.

Put succinctly, low streamwise momentum can lead to significant regions of backflow, with fluid to from the adjacent passage forming the clearance vortex. This results in a vortex core of very low total pressure, leading to large blockages and stall.

21

Design Condition   **Near Stall**
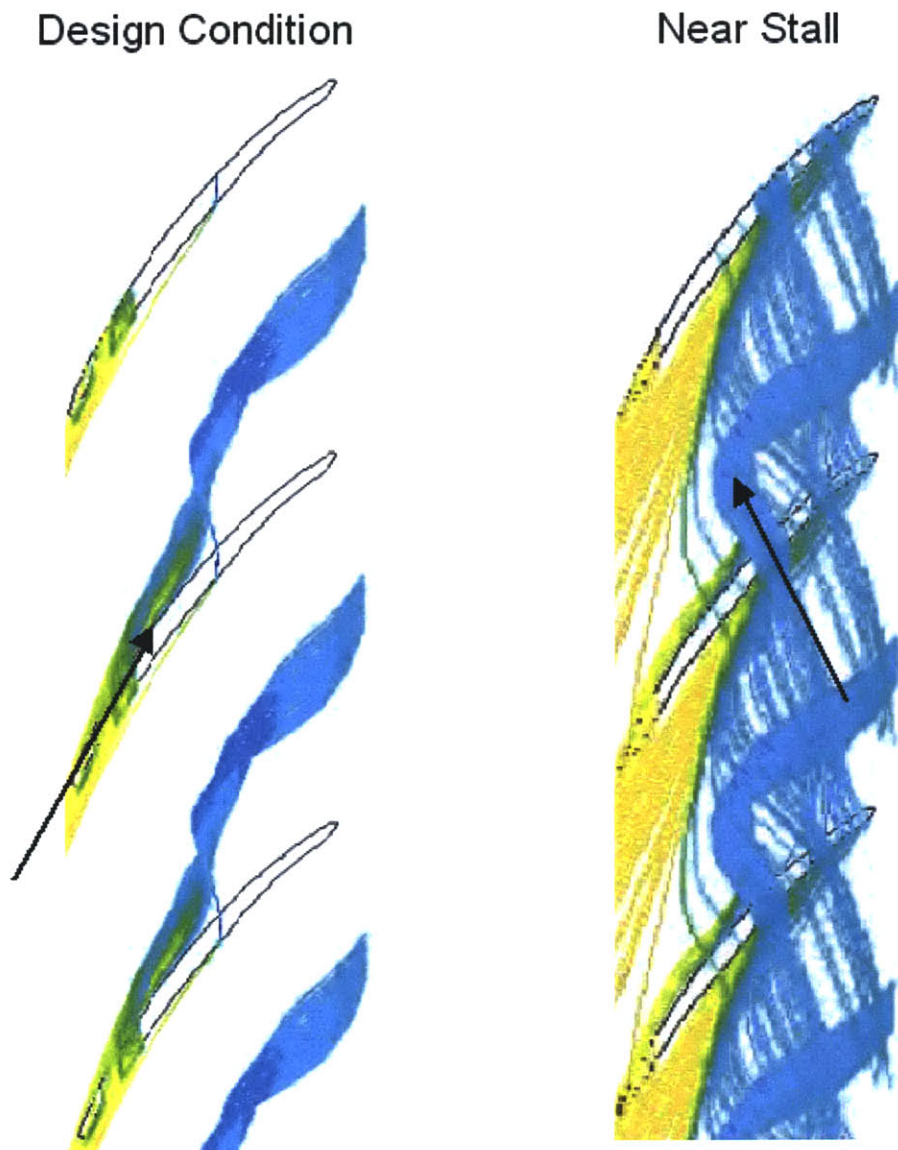
Figure 2.5 Source of Clearance Vortex Fluid. The two plots show fluid path lines of the particles that make up the vortex core. The arrows indicate from where the majority of tip clearance fluid is coming from.

2.2 Hypothesis

As stated, increasing the streamwise momentum near the blade tip has been shown to improve compressor flow range. A cause of the decrease in streamwise momentum through the blade passage is the radial transport away from the tip region. If this radial transport term can be improved, then compressor stall will be delayed. A hypothesis can thus be stated as:

- Increased streamwise momentum at the blade tip can improve compressor flow range. This fact has been highlighted by previous research, but is important in setting up the key elements of the hypothesis which follow.

- Streamwise momentum is diverted out of the blade tip region due to the radial velocity profile set up by the tip clearance vortex.

- A casing treatment geometry that helps to prevent this diversion will thus enhance the stable flow range of the compressor.

Figures 2.6 illustrates the intended effect on the flow.
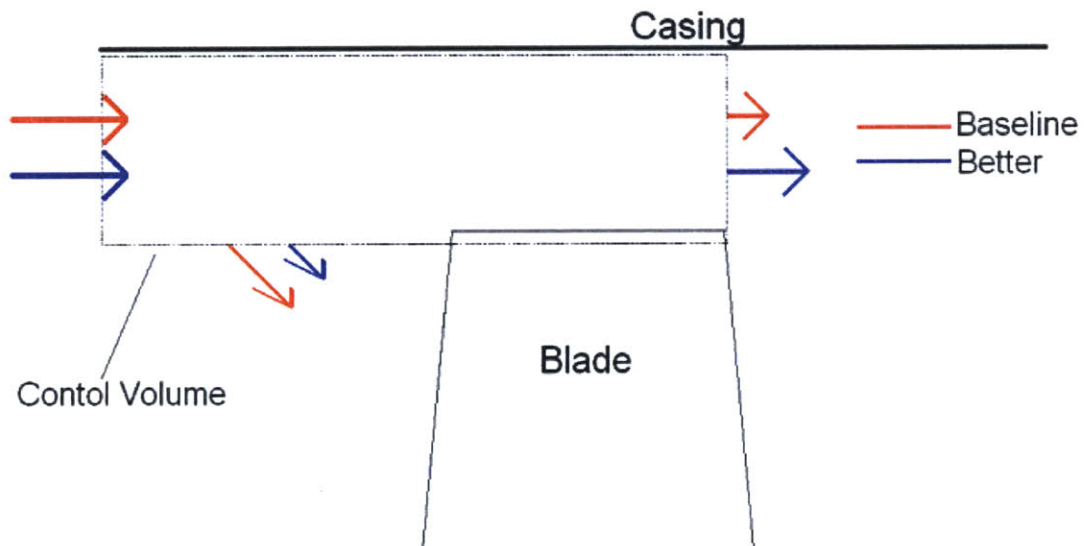
Figure 2.6 Streamwise momentum balance. The streamwise momentum via radial transport in baseline case (shown in red) is greater than with well-designed treatment (shown in blue).

Chapter 3 Technical Approach

3.1 Use of CFD

A computational approach has been used to investigate the tip clearance flow. Computational fluid dynamics (CFD) allows for effective testing and screening of a variety of casing geometries and momentum injection schemes, some of which are difficult to examine in a physical experiment. Furthermore, the flow field parameters are available everywhere in the flow, to aid interrogation. The rotor examined was the E^3 rotor B, with a 3% chord tip clearance.

In order to keep the computational cost low, single passage steady state calculations were used with a standard k-ε turbulence model. The operating point was set through varying the ratio of inlet stagnation pressure to exit static pressure. Radial equilibrium boundary conditions were applied to the exit plane, and inlet swirl (to simulate the effect of inlet guide vanes) was included as part of the inlet boundary condition.

3.2 Grid Generation

The clearance region was meshed as a separate block (this is not always a necessity, as Khalid was able to achieve accurate tip clearance flows using a periodic boundary condition on each side of the tip gap. However, to ensure capture of the clearance and casing treatment flow features, it was decided that a meshed clearance region would be used. All grids were structured in the radial direction, allowing for precise control of radial distance between cells. This is important in attaining acceptable y+ values in the

casing region, upon which turbulence modeling depends[1]. Wall functions are used so the boundary layer does not need to be full resolved in detail. For these estimates to be accurate, the cells adjacent to the wall must be within a specific range of y+ values.

Although the density of cells in the vicinity of the blade surface is not as great as in the tip region (Figure 2.7), this should not affect the results appreciably. This compressor row has been shown by Vo [19] to be tip limited, so the flow over the main portion of the blade surface is healthy and not as crucial to stall onset.

Ideally, the solution should be independent of the grid resolution. Given the number of grids and geometries that were tried, this is difficult. However, solutions from different grids indicate that difference in results (flow range, pressure rise, efficiency) due to grid change is still less than the differences due to the experimental changes (momentum injections, geometry changes) that were being tested.
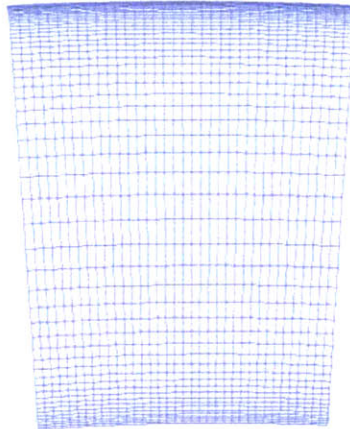
Figure 3.1 Radial variation in grid density, showing high density in the tip region.

---

[1] This value is simply a non-dimensional disance, defined as

$$y^+ = \frac{\rho u_\tau y}{\mu}. \tag{2}$$

3.3 Use of Numerical Stall as Flow Range Indicator

The relationship between steady-state numerical stall and physical stall is critical to this study. The type of numerical calculations done were single-passage, steady state calculations. The point at which numerical stall occurs in these calculations will be referred to as the equilibrium point. Past the equilibrium point, a solution for the flow conditions specified cannot be found, and the flow field becomes progressively further from a solution, with the residuals showing a sharp increase[2]. More importantly, the equilibrium point coincides with a sharp rise in the production of tip blockage. Physical stall is also associated with a sharp increase in the blockage level in the vicinity of the stall point. While this gives some plausibility to the relationship between the equilibrium point and the physical stall point, it by no means links them clearly.

In his thesis, Vo [19] performed both steady and unsteady calculations to compare the equilibrium point found in steady state calculations with physical stall point found in the unsteady calculation. He found that changes in equilibrium point follow the trend that occurs with physical stall point. In other words, if something is done to the flow field that delays the equilibrium point, evidence indicates that the change will occur for the physical stall.

---

[2] The residuals are a measure of how well the calculation satisfies the defining equations (continuity, Navier-Stokes, etc.). Large residuals indicate that computation is not accurate.

Chapter 4.0 Assessment of the Hypothesis

4.1 Body Forces as a Diagnostic

The use of body forces within the flow, or massless momentum injection, provides one way to test the hypothesis put forth in Chaptern2. In the implementation, the direction of the applied force is specified so that it remains perpendicular to the relative velocity and the relative total pressure is unaffected by the force. The local force per unit volume magnitude is scaled with the local relative velocity magnitude, as in equation 3.

$$Force/volume = C \bullet V'$$ (3)

The constant 'C' can be changed to vary the strength of the body force. Two cases are described below. In one, the constant was chosen so that the total body force was approximately 0.3 percent of the blade force. This value was chosen because initial casing treatment calculations indicated the magnitude of the force of the grooves on the flow is approximately 0.3 percent of the blade force. This setup will be referred to as "Casing Force (low)". "Casing Force (high)" refers to the setup when the total body force was approximately 0.9 percent of the blade force.

These specifications of the characteristics of the body forces were implemented through a user-defined function such that the body forces were updated after every iteration. This code for the user-defined function can be found in Appendix A. Fig. 4.1 shows the region in which the force was applied. The momentum injection was applied at different locations, but the following detailed interrogation is associated with only one region of application; this position provides the greatest benefit and insight into the best way to alter the flow in order to improve flow range.
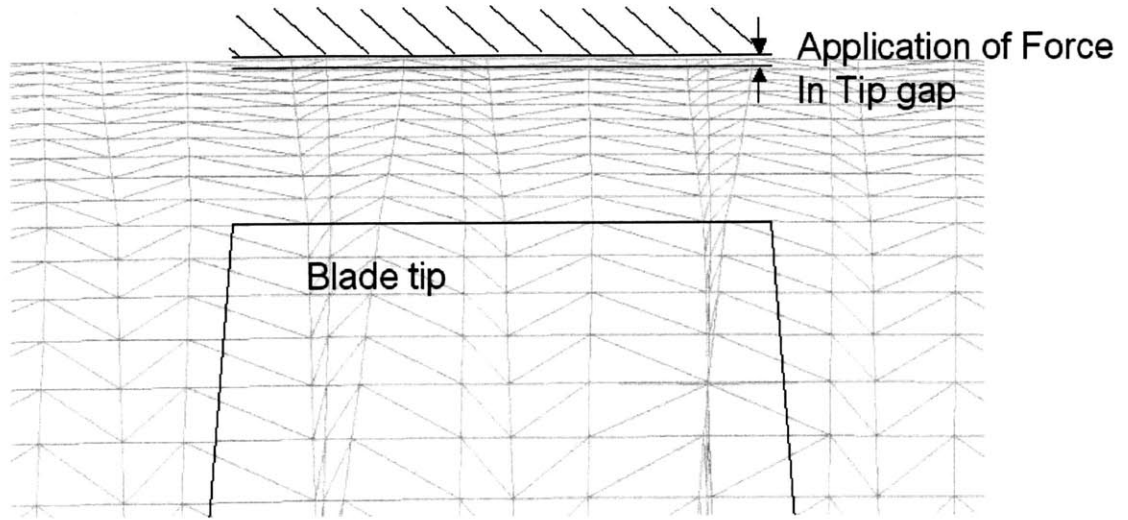
Figure 4.1 Sketch of geometric c configuration of tip flow region indicating location of body force application

4.1.2 Results

Figures 4.2 and 4.3 show the results of pressure rise coefficient and efficiency for the baseline (no force), casing force (low), and casing force (high). The pressure rise coefficient used is the total-to-static pressure rise, as shown in equation 4.

$$\text{Pressure Rise Coefficient} = \frac{P_2 - P_{t1}}{0.5\rho U^2_{tip}} \qquad (4)$$

Station 1 is a 10% of the blade tip axial chord upstream of the blade passage, and station 2 is 10% downstream of the blade passage. Static pressures are area-averaged, and stagnation pressures and temperatures are mass-averaged. The definition for adiabatic efficiency is shown in equation 5 below.

$$\text{Adiabatic Efficiency} = \frac{\left(P_{t2}/P_{t1}\right)^{\frac{\gamma-1}{\gamma}} - 1}{\left(T_{t2}/T_{t1}\right) - 1} \qquad (5)$$

The flow coefficient is the area-averaged axial velocity at the inlet normalized by the blade tip speed.

$$\phi = \frac{u_x}{U_{tip}} \qquad (6)$$

Figures 4.2 and 4.3 indicate that the body force has resulted in a flow range extension, an increased peak pressure rise, and increased peak efficiency compared to the baseline case. Furthermore, the improvements increase as the magnitude of the body force increases.
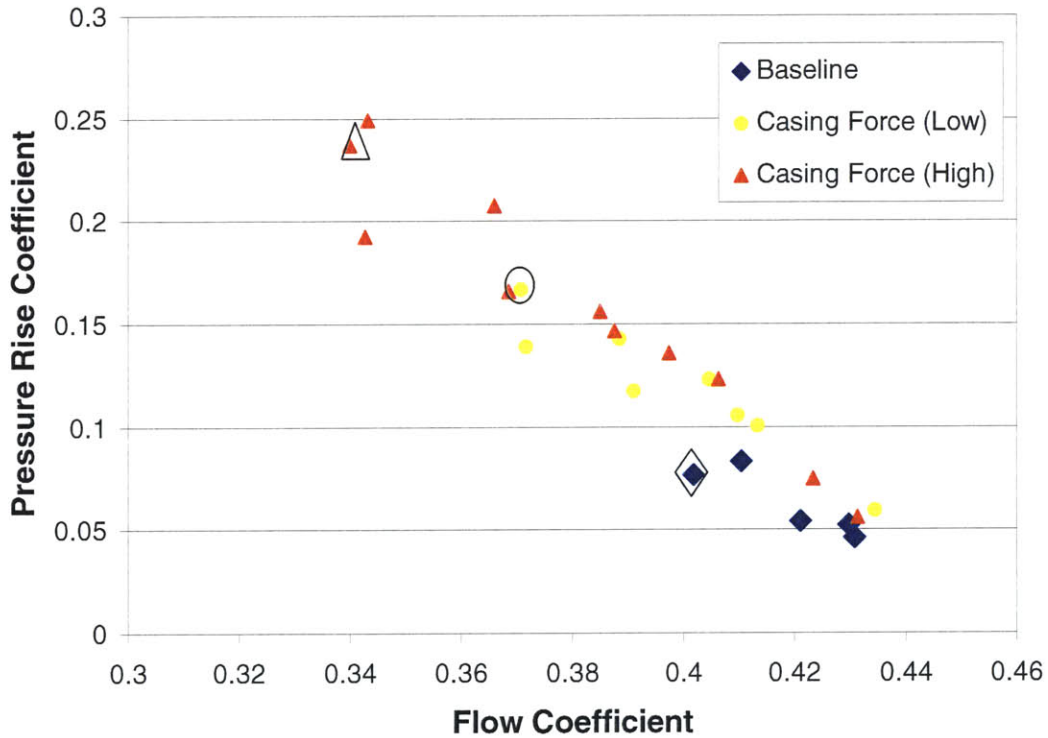
Figure 4.2 Pressure rise coefficient vs. flow coefficient. The equilibrium point of each case is marked with a dark encirclement.
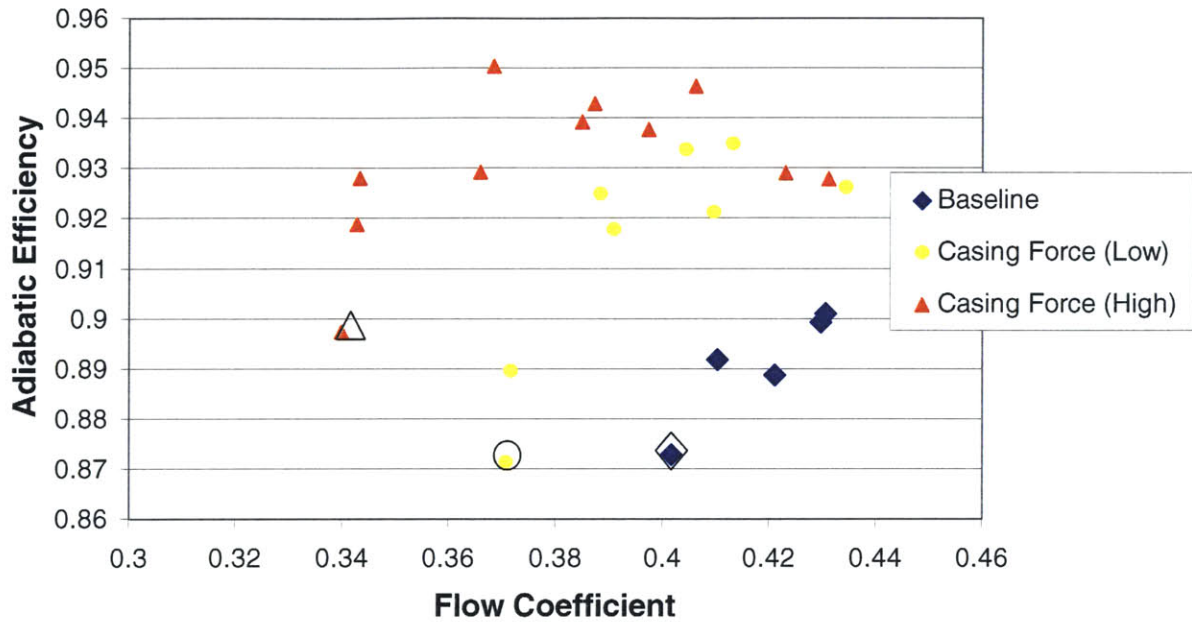
Figure 4.3 Adiabatic efficiency vs. flow coefficient

As discussed in Chapter 2, increased streamwise velocity within the blade passage at the blade tip level results in improved flow range, peak pressure rise, and peak efficiency. One can expect that the streamwise velocity in the tip region is greater with the body force. This is confirmed in the streamwise velocity contours evaluated at the blade tip level, which are shown Figures 4.4.

4.1.3 Changes in Radial Transport

The results show that a small force acting near the casing wall produces a large change close to the blade tip, and improves the flow range. To understand this influence, we first look at the baseline case. We consider the radial flux of streamwise momentum
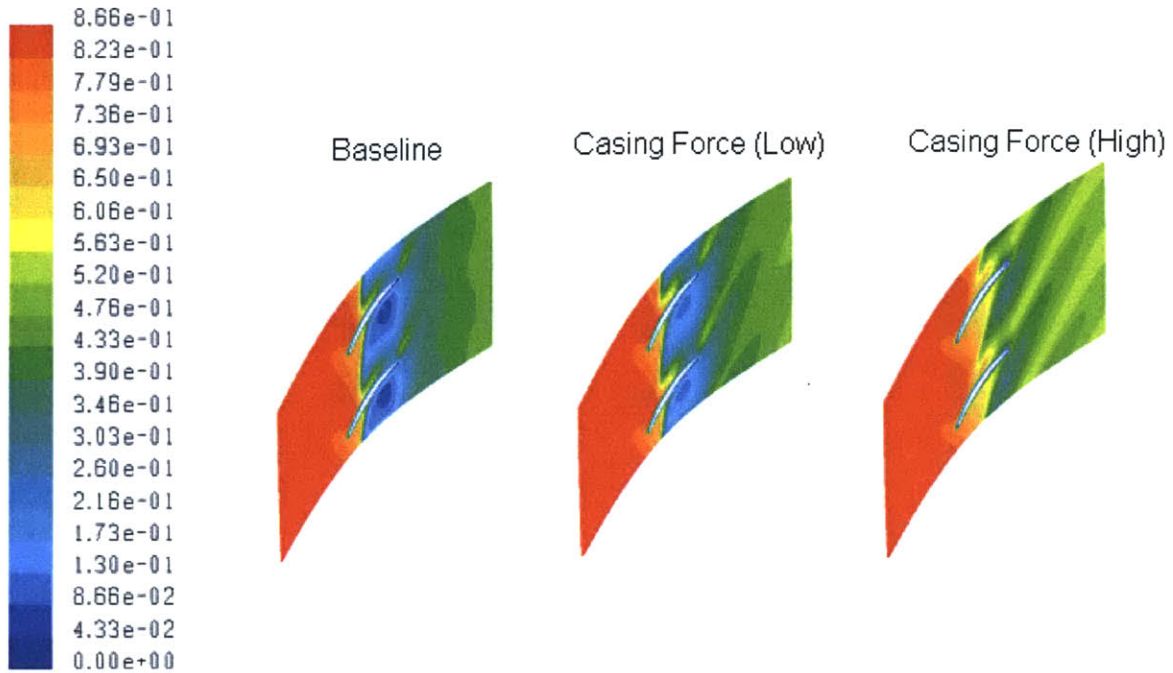
Figure 4.4 Streamwise velocity contours at 100% span. The values shown are streamwise velocities normalized by the blade tip speed.

Evaluated at the tip location, as defined in equation 7. The integration is carried out over one blade passage.

$$\text{Normalized Radial Transport of Streamwise Momentum} = \frac{\left.\iint\limits_{100\%} \rho u_r u_s dA \middle/ \tau\right.}{\left. Force_{blade} \middle/ (r_t - r_h)\right.} \qquad (7)$$

The flux per tip clearance distance is 1.4 times the blade force per unit blade span, which means near the blade tip this flux is of similar importance as the blade force. This is a result of the velocity associated with the tip clearance vortex, as shown by the following. The radial velocity can be estimated using a potential flow model of the tip clearance vortex. As shown in figure 4.5, the clearance vortex was estimated as a straight line vortex in the tangential direction. The circulation of the model vortex is taken to be equal to the average circulation of the actual vortex.

31

Figure 4.6 shows the potential theory estimate and the CFD results of the radial velocity at 100% span. The figure shows good agreement in the radial velocity profile, especially in the first half of the blade passage. Towards the trailing edge, the potential theory model diverges from the CFD result because the former does not account for the effects of blockage that occurs near the trailing edge. The main point, however, is that the tip clearance vortex is responsible for the large inward radial velocity near the leading edge.
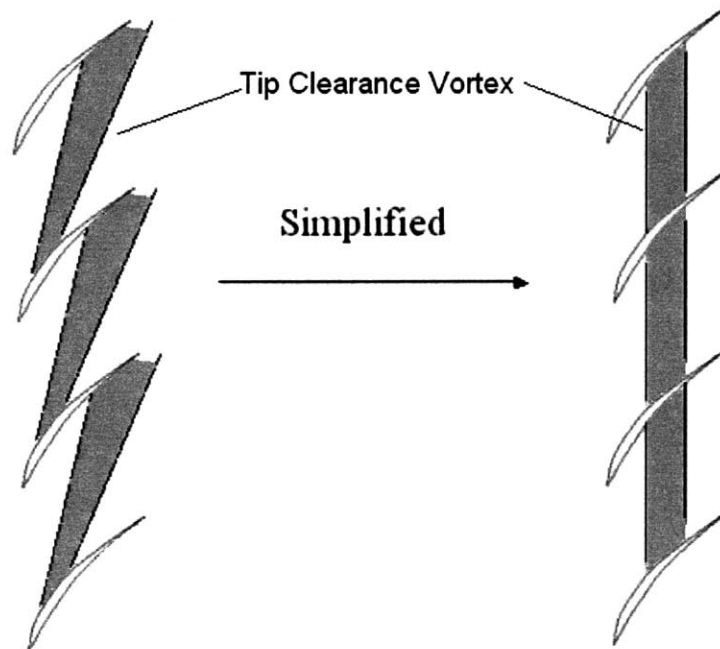
Figure 4.5 Vortex simplification. The complex geometry and trajectory of the tip clearance vortex is modeled as a simple straight vortex in the tangential direction.

The body forces reduce the effect of the tip clearance vortex on the radial velocity profile. The radial transport of streamwise momentum leaving the tip region is thus lessened. This occurs because the non-conservative body force creates a vortex counter to the tip clearance vortex (see Figure 4.7), essentially reducing the strength of the clearance vortex.
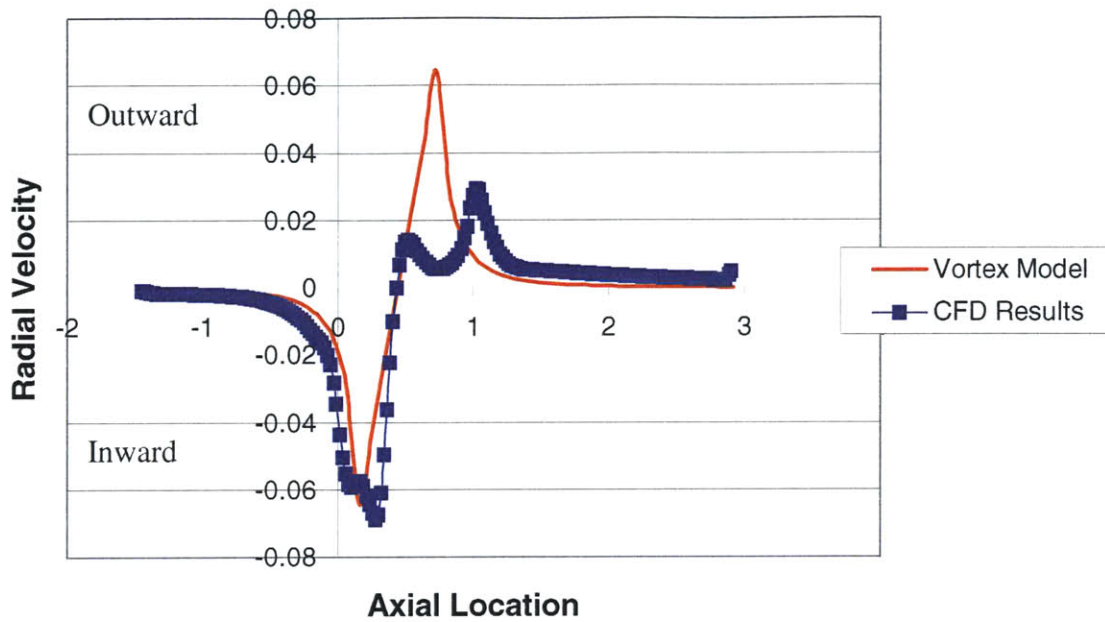
Figure 4.6 Pitchwise-averaged radial velocity vs. axial location, measured at the blade tip. x=0 represents the blade tip leading edge and x=1 is the trailing edge location
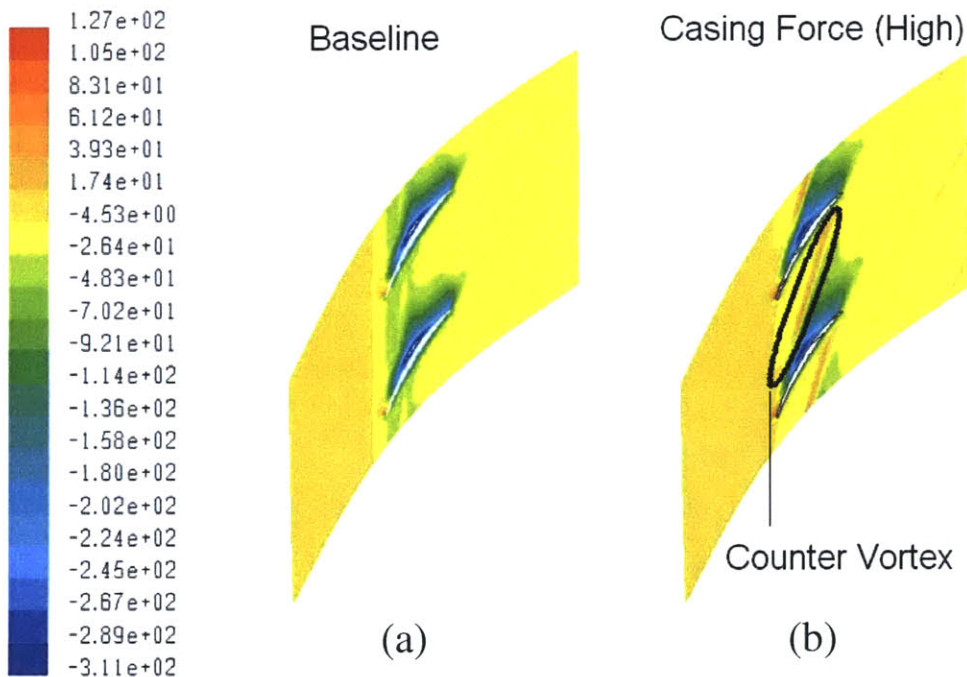
Figure 4.7 Tangential vorticity at 100% span. Values normalized by angular velocity. The presence of the body force generated counter vortex is indicated in (b), compared to the baseline case in (a)

Key properties associated with the use of the body force are shown in Table 1.

The change in the radial transport term (as given in equation 7) is the primary factor

associated with the improvement of streamwise momentum at the blade tip. Since the

measurement is made on a two-dimensional plane at 100% span, streamwise velocity is

parameter measured. The streamwise velocity is area-averaged at 100% span within the

axial extent of the blade passage and normalized by the blade tip speed (equation 8,

below).

$$\text{Streamwise Velocity} = \frac{\left[\left(\frac{1}{A_{BP100\%}}\right)\iint_{BP100\%}u_s dA\right]}{U_{tip}} \qquad (8)$$

The flow range extension is defined as the fractional change in the stall flow coefficient,

or

$$\text{Flow Range Extension} = \frac{\phi_{s,new} - \phi_{s,baseline}}{\phi_{s,baseline}} \qquad (9)$$

The change in streamwise momentum retained in the endwall region through change in

radial transport term is about 5 times greater than the body force. The implication is that

the direct effect of momentum injection is not as important as the associated changes to

the flow field.

Table 1 Key properties at the baseline stalling flow coefficient.

	Radial Transport Term	Streamwise Velocity	Flow Range Extension
Baseline	-1.397	0.530	0
Casing Force (Low)	-0.988	0.625	0.077
Casing Force (High)	-0.619	0.676	0.154

Pitch-Averaged radial velocity and radial transport profiles show how the streamwise momentum is more effectively retained near the blade tip with the body force than in the baseline situation. With the body force the radial velocity magnitudes are greatly reduced, particularly the large negative spike near the leading edge (see figure 4.8). These radial velocities are linked closely with the radial transport of streamwise momentum, as depicted in figure 4.9.
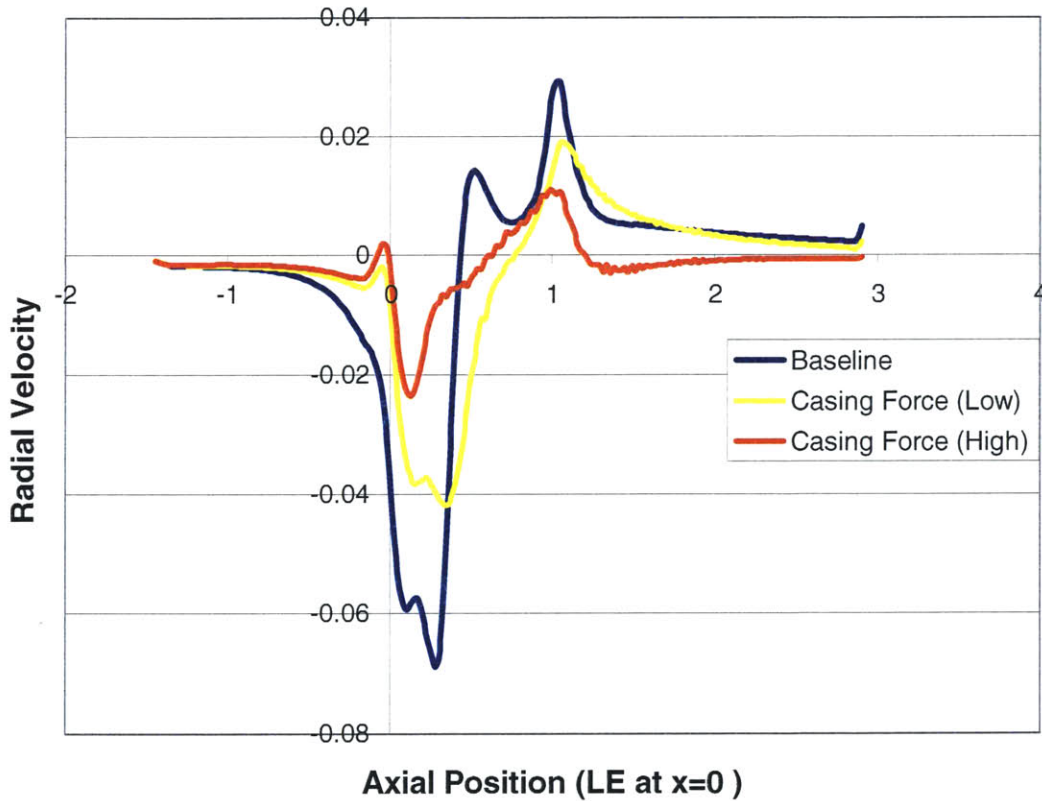
Figure 4.8 Pitchwise-averaged radial velocity vs. axial position. Radial velocity normalized by the blade tip speed. The leading edge of the blade tip is located at x=0. The trailing edge is located at x=1.
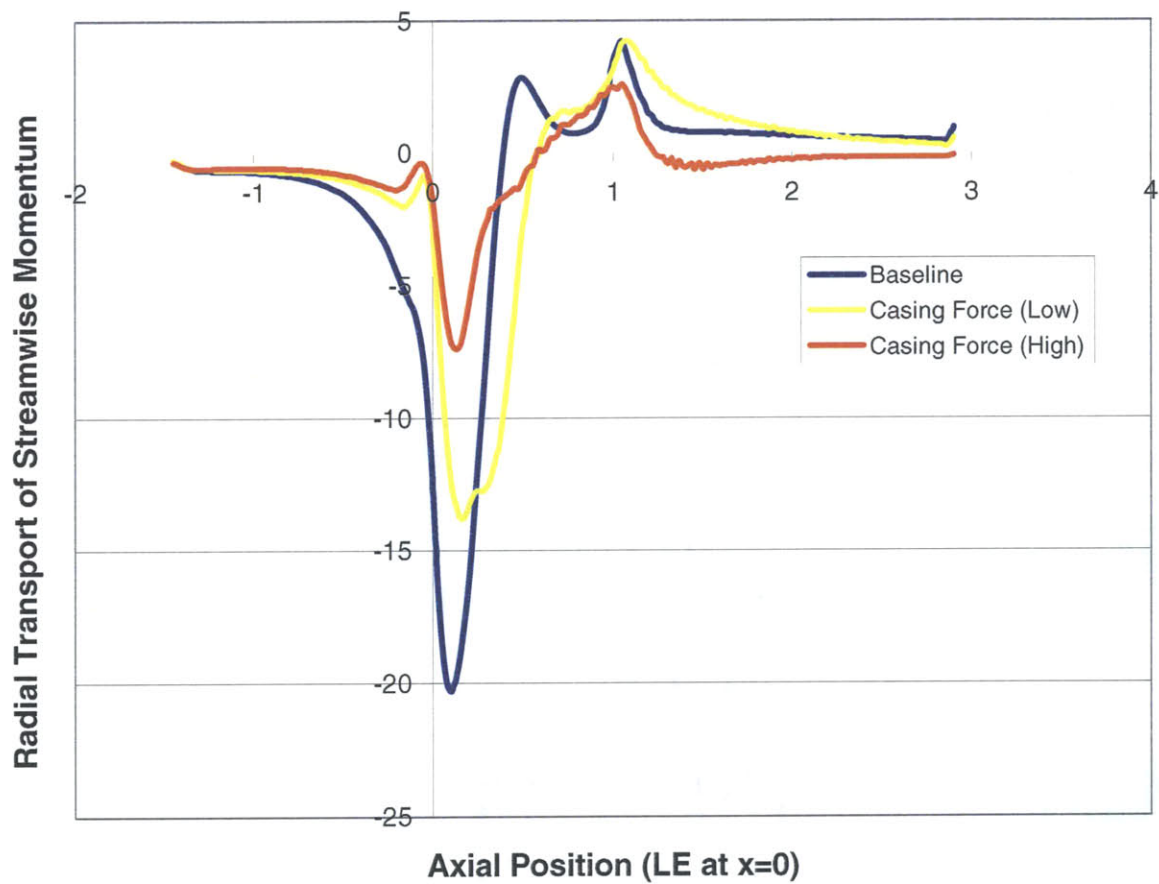
Figure 4.9 Pitchwise-averaged radial transport of streamwise momentum vs. axial position. Radial Transport normalized by the blade force per unit blade area. The leading edge of the blade tip is located at x=0. The trailing edge is located at x=1.

4.2 Use of a Flat Plate at the Blade Tip as a Diagnostic

Another set of simulations which support the hypothesis is provided by the insertion of a plate into the compressor flow upstream of the blade, as shown in figure 4.10. No flow can pass through the plate. As described below, it is found that more streamwise momentum is retained in the tip region than in the baseline situation.

Casing
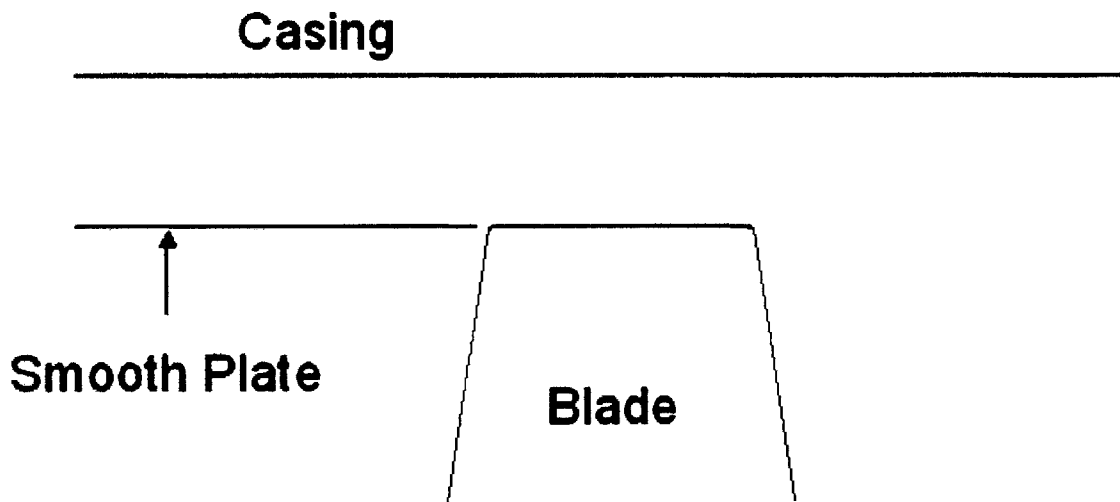
Figure 4.10 Setup of plate in stream experiment

4.2.2 Results

The results of the experiment with the plate can be seen in figures 4.11 and 4.12. The presence of the plate resulted in greater flow range, greater peak pressure rise, and greater efficiency compared with the baseline. The results from the low casing force are also included comparison. The radial transport term, streamwise velocity, and flow range of the experiment can be seen in Table 2. The plate lessens the magnitude of the radial transport term and increases streamwise momentum at the blade tip (relative to the baseline case).
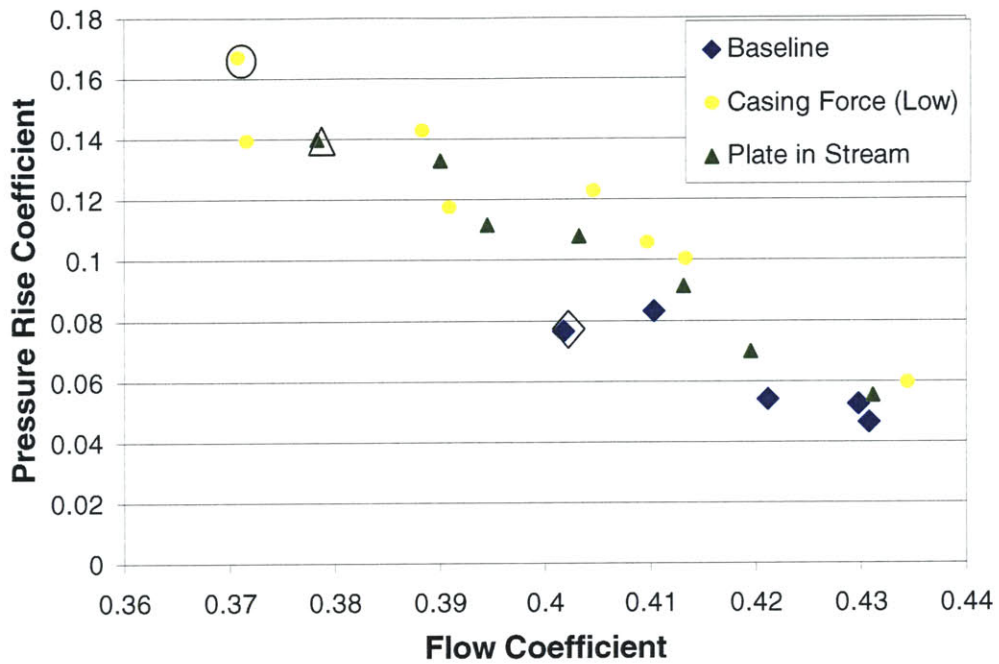
Figure 4.11 Pressure rise coefficient vs. flow coefficient. The presence of the plate improves flow range, peak pressure rise.
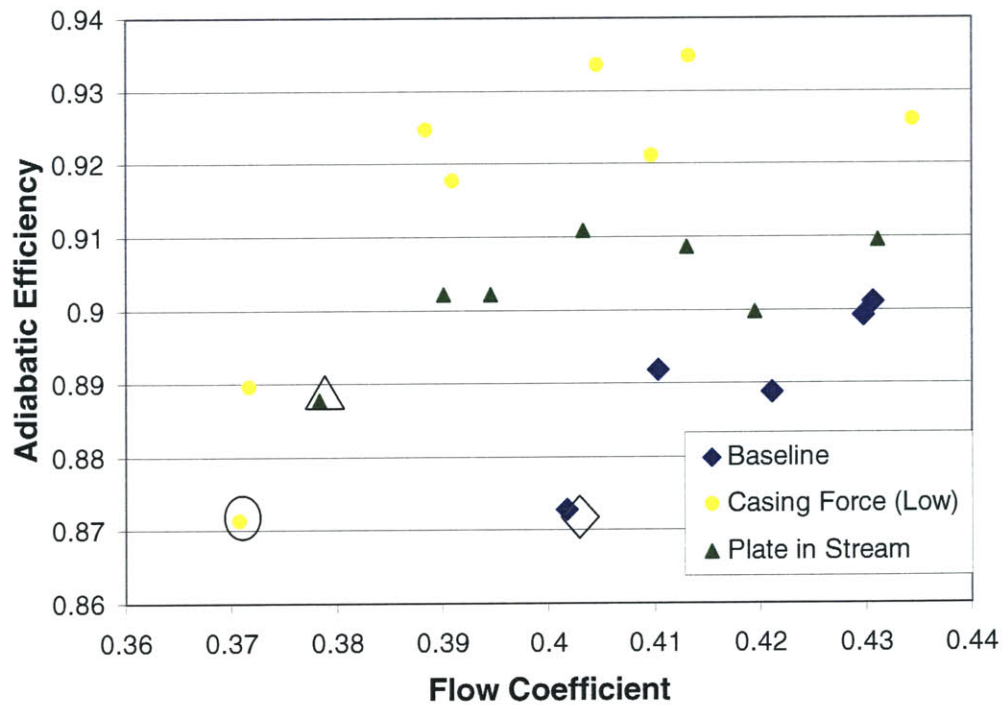
Figure 4.12 Adiabatic efficiency vs. flow coefficient. The presence of the plate increases peak efficiency.

38

Table 2. Key properties at baseline stalling flow coefficient.

	Radial Transport Term	Streamwise Velocity	Flow Range Extension
Baseline	-1.397	0.530	0
Casing Force (Low)	-0.988	0.625	0.077
Plate in Stream	-0.984	0.591	0.059

4.2.3 Changes in Radial Transport

Figure 4.13 shows the radial velocity profile at 100% span. The profile is not changed within the blade passage. Only upstream of the blade passage is the radial velocity at 100% span brought to zero. This control of the radial velocity, even within the limited axial extent, leads to greater retainment of streamwise momentum within the tip region, as seen in figure 4.14.

The simulation with the plate shows an improvement in flow range without direct streamwise momentum injection. Rather, it is due to alteration of the radial velocity profile[3]. These results, which provide support that the improvement is obtained by changing the radial velocity profile, also provide a stepping-stone to understanding of casing treatment.

---

[3] There is a small direct streamwise force by the plate on the flow. In the same way that an axial flow can exert a force on an engine inlet, the streamlines curving around the leading edge of the plate cause a net pressure force to act on the plate [7]. However, this force is more than two orders of magnitude smaller than the total change in the radial transport term seen with the plate. Therefore, it is unlikely that this effect is important.
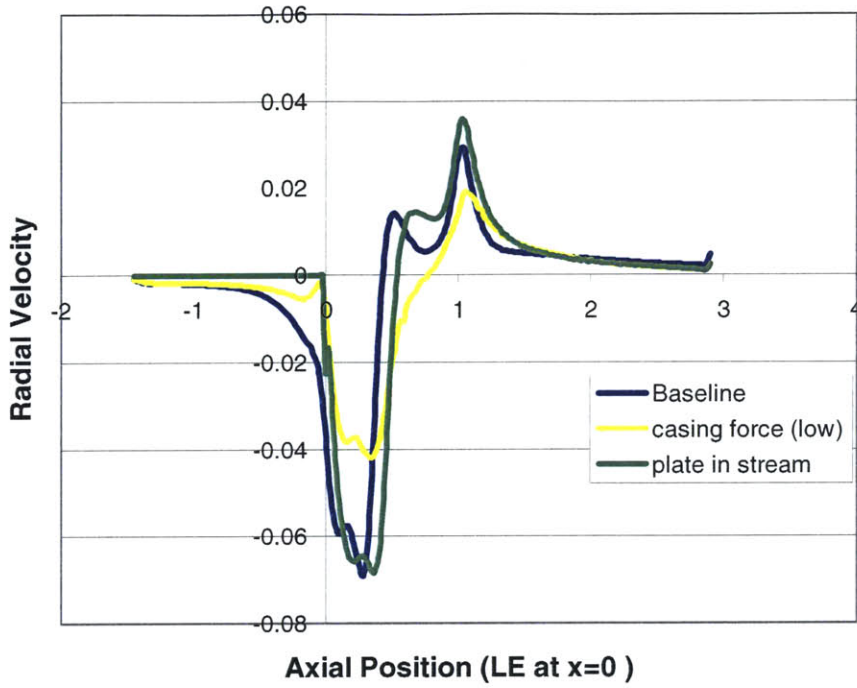
Figure 4.13 Pitchewise-averaged radial velocity vs. axial position. The presence of the plate
preventes radial velcity upstream of the blade.
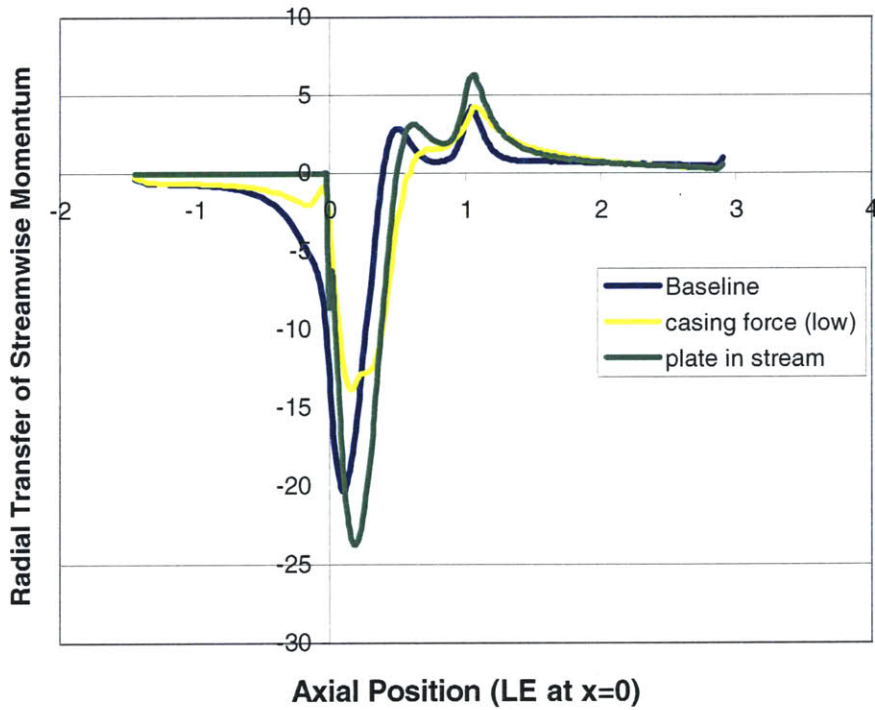
Figure 4.14 Pitchwise-averaged radial transport of streamwise momentum vs. axial position. The presence
of the plate prevents radial transport upstream of the blade.

Chapter 5 Casing Treatment

5.1 Setup

One goal of this research is to link flow changes that result in enhanced flow range with practical casing treatment geometry. The casing treatment configuration examined consisted of a single shallow circumferential groove located at the quarter chord of the blade passage. The choice of geometry was made after consideration of previous research pertaining to circumferential grooves. Two major geometrical factors were number and depth of grooves. Adamczyk and Shabbir [2] and Rabe and Hah [15] found that the most benefit is achieved from the grooves near the leading edge. Rabe and Hah tried different groove depths and showed that the groove depth necessary to affect substantial change only needs to be on the order of the clearance gap. For this reason, only one groove near the leading edge was used, and the maximum groove depth was equal to the clearance gap. Shallower groove depths were examined in order to determine how the performance approached the smoothwall performance as the depth approached zero. The geometry of the groove treatment is shown in Fig. 5.1.

5.2 Results

The pressure rise coefficients and efficiencies resulting from the casing treatment numerical experiments are shown in figures 5.2 and 5.3. The percentage given before each data set tells how deep the groove is relative to the tip clearance (i.e. 100% is equal to the tip clearance). Circumferential treatment of groove depths tried resulted in improved flow range, greater pressure rise, and greater efficiency.

41

The computed results were assessed against those of Adamczyk and Shabbir [2], who also investigated a low speed rotor with circumferential groove type casing treatment. The result from their work is reproduced in Figure 5.4. The change in

Side View

Flow Direction

Top View

Groove ———

Blade ———
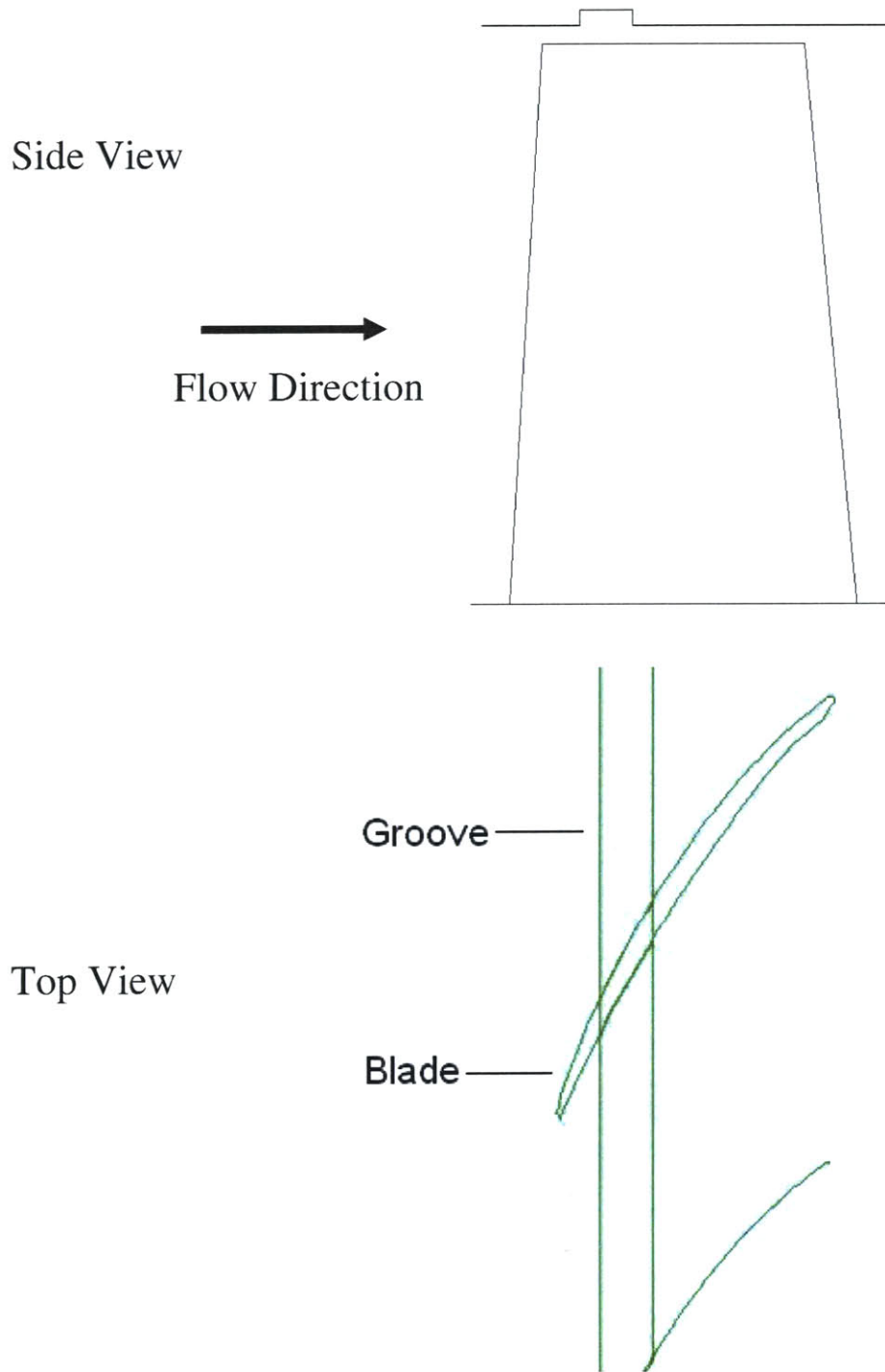
Figure 5.1 Views of the casing treatment geometry
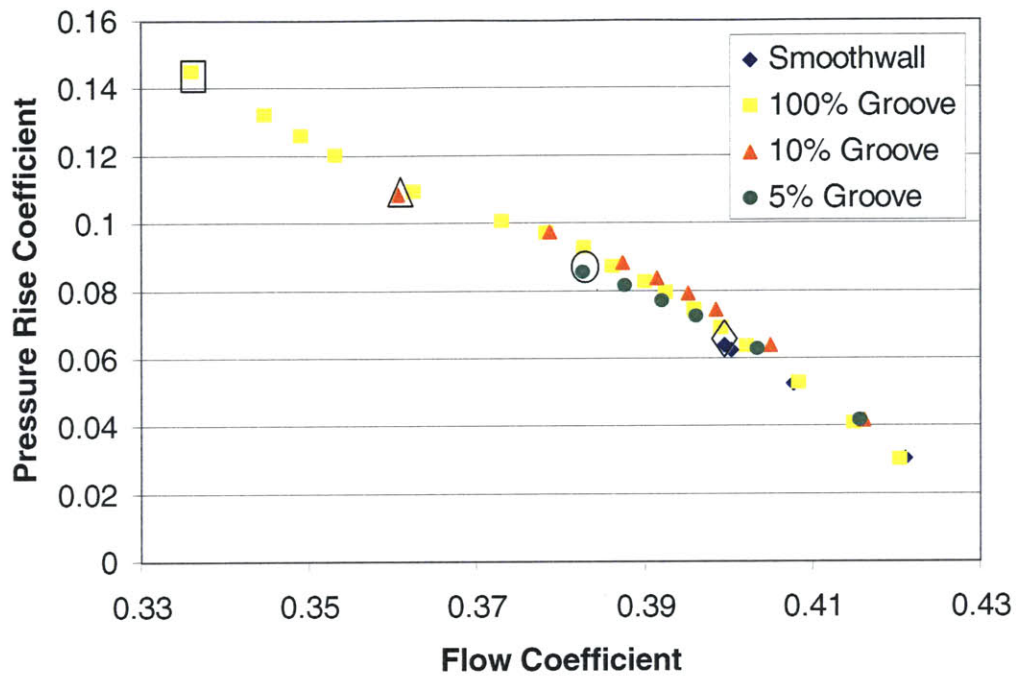
Figure 5.2 Pressure rise coefficient vs. flow coefficient. The casing treatment improves flow range and peak pressure rise.
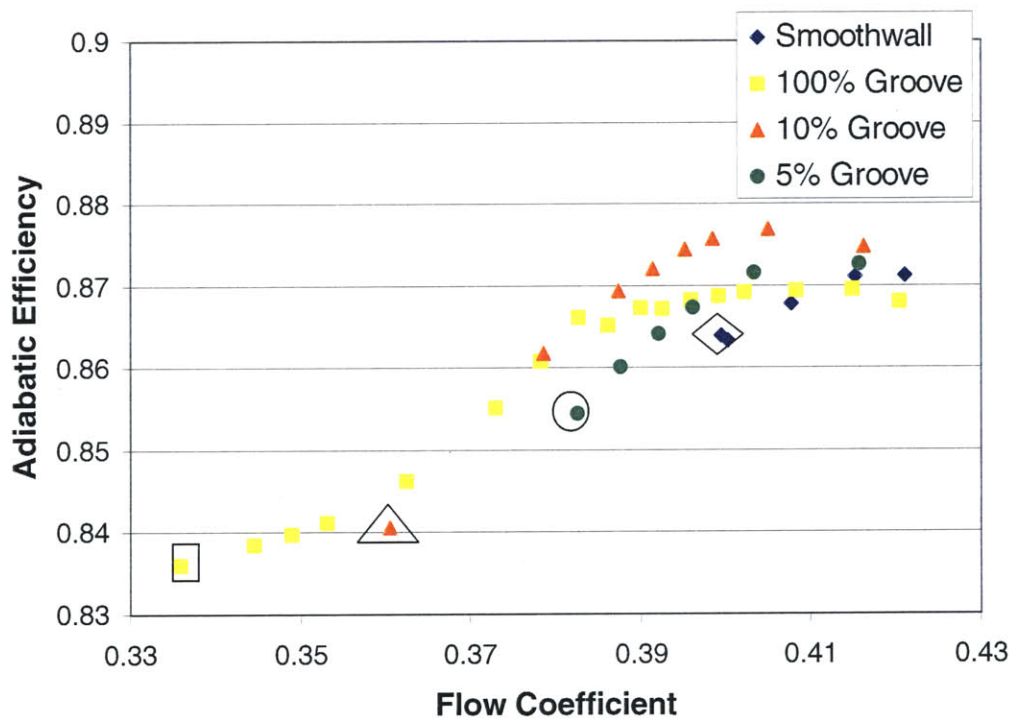
Figure 5.3 Adiabatic efficiency vs. flow coefficient. The casing treatment improves efficiency.
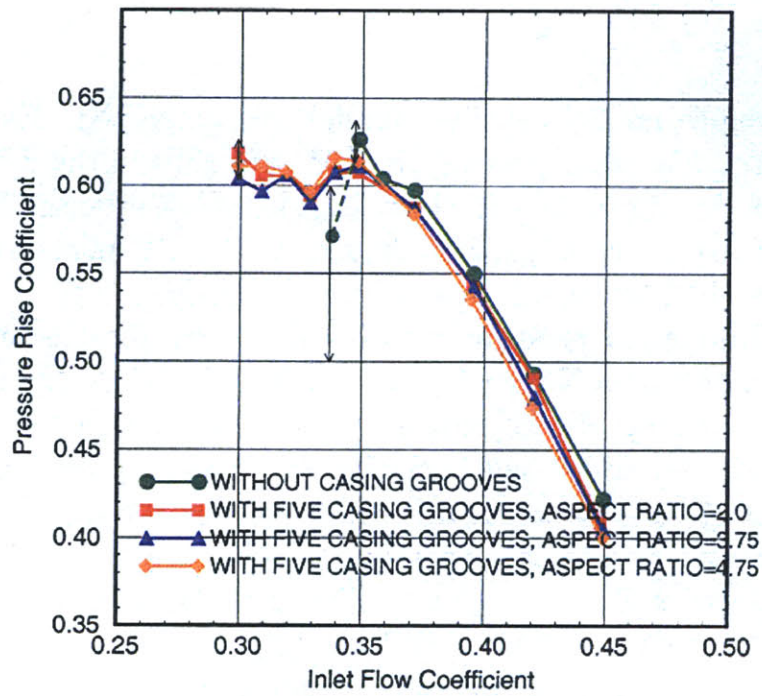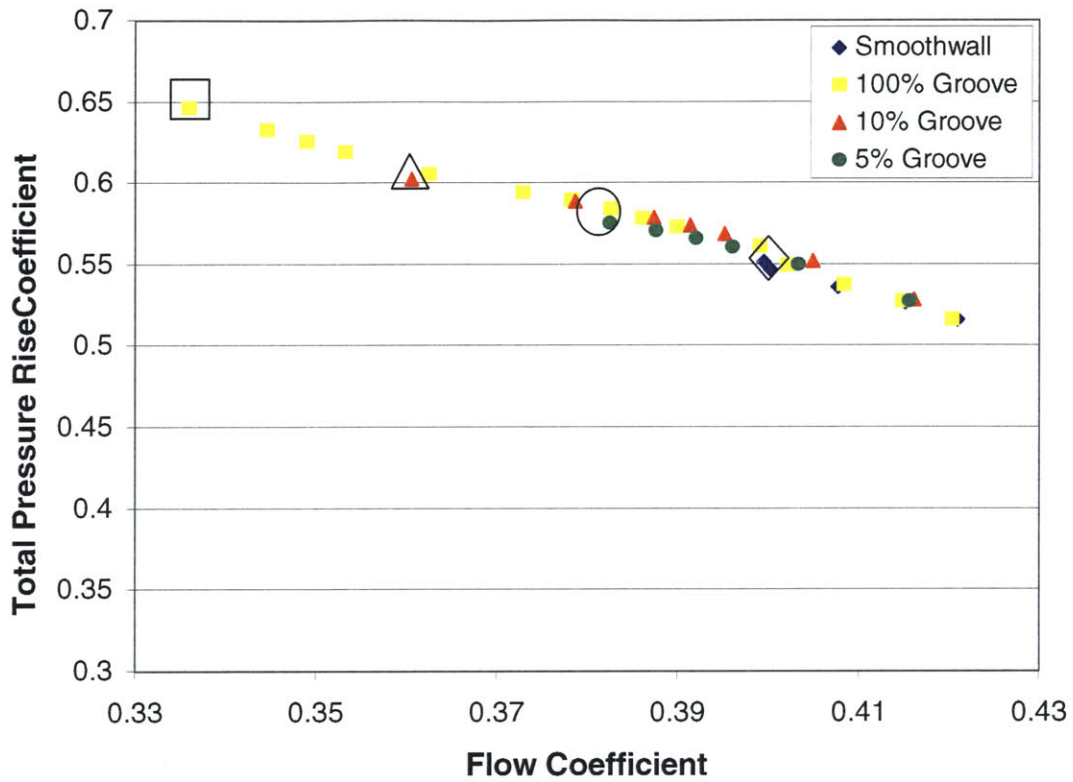
Figure 5.4 Total pressure rise coefficient vs. flow coefficient as calculated by Adamczyk and Shabbir [2] (bottom), compared with calculations of this research (top).

the computed stall flow coefficient achieved by Shabbir, et al. was 14.3%, compared to 16.0% for the case of the 100% groove described here, for similar (not identical rotors). The details of the flow will now be examined to determine how flow range has been extended.

5.3 Changes in Radial Transport Term

As with the previous methods of flow field alteration, the major effect of the casing treatment is seen as mitigating the radial transport of streamwise momentum out of the tip region, especially in the leading edge region. Continuity (for an incompressible flow) dictates that the average radial velocity at the groove entrance is zero. However, the circumferential groove can affect the distribution of radial velocity. This is important because of the distribution of streamwise velocity at the blade tip. Figure 5.5 shows the change in streamwise velocity is a result of radial transport and diffusion. Radial velocities near the leading edge affect the radial transport more than velocity changes at the trailing edge. Therefore, if the radial velocity profile is altered so that there is an increase in radial velocity at the leading edge and a decrease near the trailing edge, the total radial transport of momentum can be reduced, even though the average radial velocity is the same.
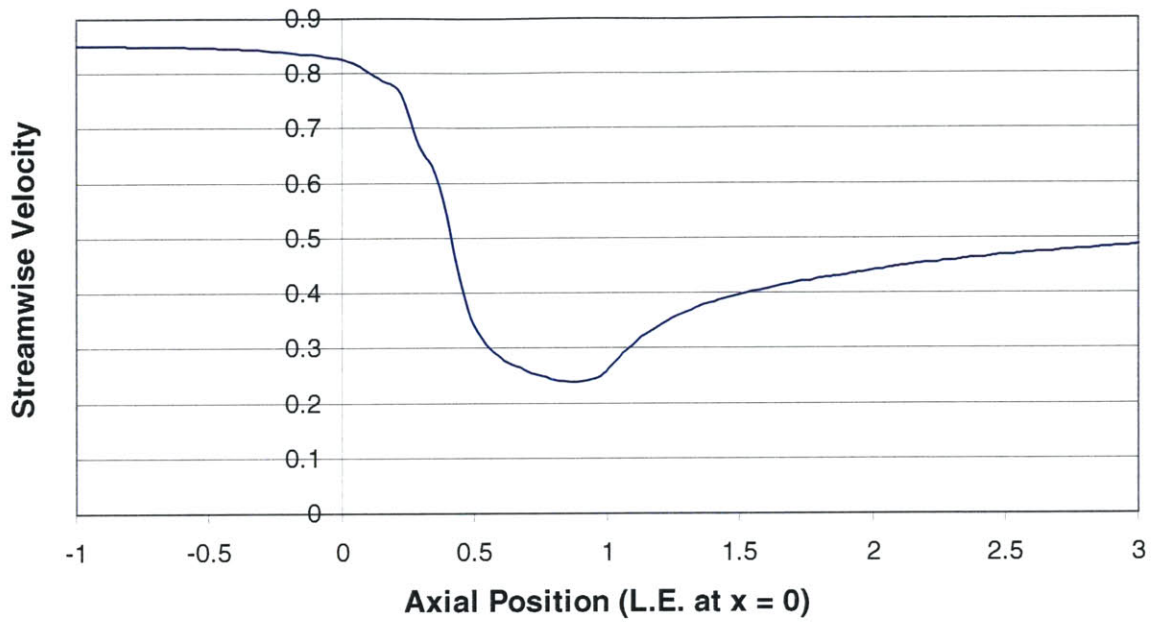
Figure 5.5 Pitchwise-averaged streamwise velocity vs. axial position. Measurement taken from smoothwall case near stall at 100%span. L.E. at x=0. T.E. at x=1.
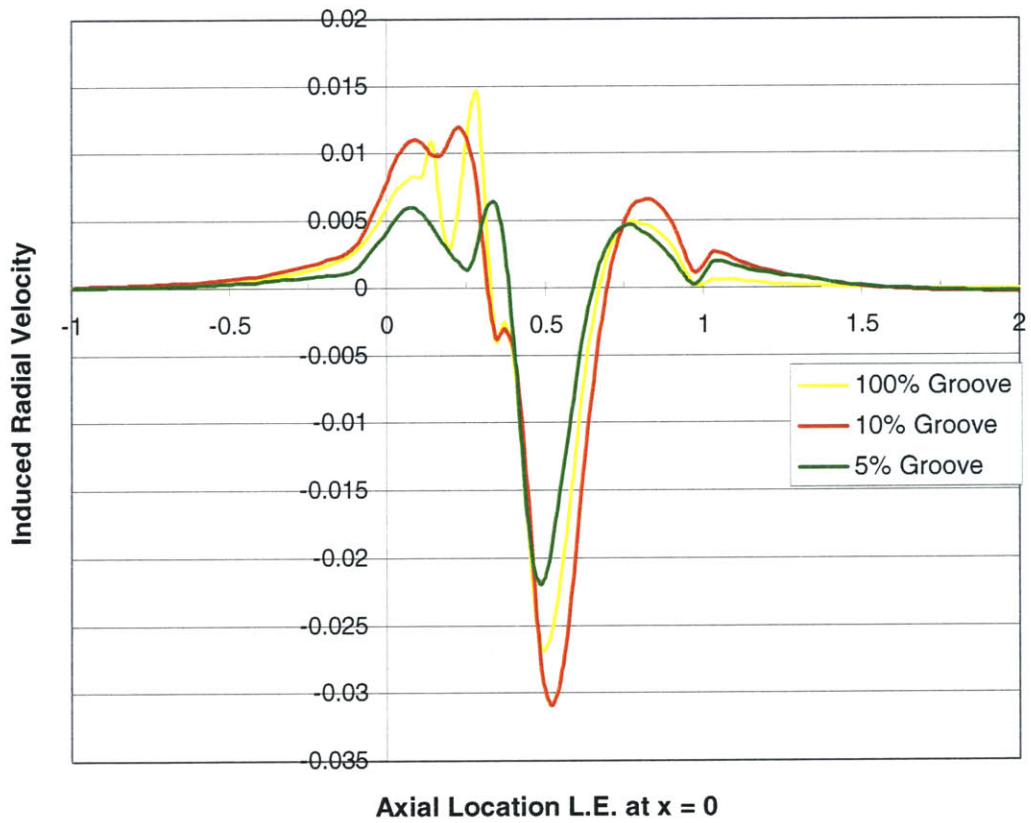
Figure 5.6 Pitchwise-averaged induced radial velocity vs. axial location, measured at 100%span.

The induced radial velocity is defined as the difference in radial velocity between the casing treatment and the smoothwall case. Figure 5.6 shows the induced radial velocity profiles of the circumferential groove casing treatments. There is a large positive induced velocity near the leading edge, which is responsible for the improvement in the radial transport of streamwise momentum.

To isolate the dominant mechanism proposed for the enhancement of streamwise momentum, we can also examine the change in shear force on the flow, the flux of streamwise momentum out of the groove, and the pressure force using the control volume shown in Fig. 5.7. The changes in each term are listed in Table 3. The terms are listed as force per unit span, normalized by the blade force per unit blade span. The radial
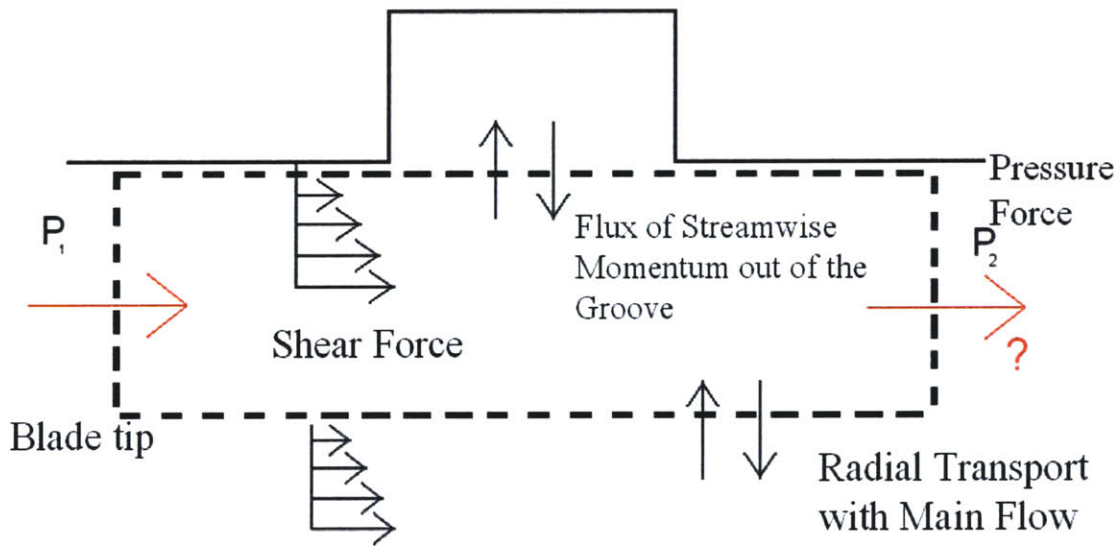
Figure 5.7 Control volume used in momentum balance

Table 3 Magnitudes of streamwise momentum terms

	Pressure	Shear	Groove Flux	Radial Transport
100% Groove	-0.909	-0.179	0.005	-1.126
Smoothwall	-0.902	-0.166	0	-1.178
Difference	-0.007	-0.013	0.005	0.052

transport term constitutes the largest difference. In fact, the pressure force and shear forces on the control volume slightly worsen use of casing treatment. We can infer that the change in streamwise momentum at the blade tip is primarily a result of changes in radial transport. Table 3 confirms the radial transport of streamwise momentum is the dominant term that is altered by the application of circumferential groove type casing treatment.

Calculations with different groove depths show an optimum groove depth for achieving the best peak efficiency, and which is smaller than the clearance gap. In terms of flow range extension and peak pressure rise, however, grooves with greater depth perform better, although a 50% groove showed nearly identical flow range improvement as the 100%. The 50% groove calculations were examined specifically to show that flow range improvement increases with groove depth, but the improvement asymptotically approaches a maximum. These characteristics are illustrated in figure 5.8.

The qualitative effect of the groove changes the flow coefficient. At high flow coefficients, for instance, there is a slight reduction in flow range with the 100% groove (i.e. groove depth = tip clearance) compared to the smoothwall case. The computed groove-induced radial velocity (at flow coefficient near the smoothwall design) shown in figure 5.9 show that velocity profile has not been altered in a manner which improves radial transport.
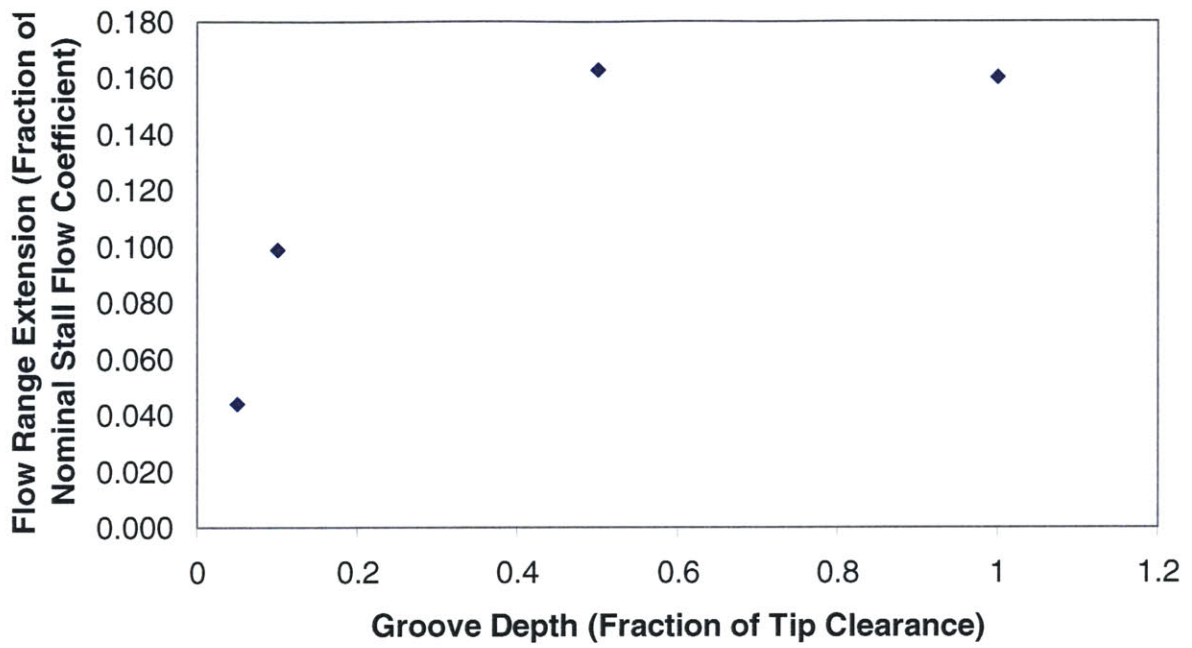
Figure 5.8 Flow range extension vs. groove depth.   Flow range improvement asymptotically approaches a maximum as groove depth is increased.

Axial Position (L.E. at x = 0)
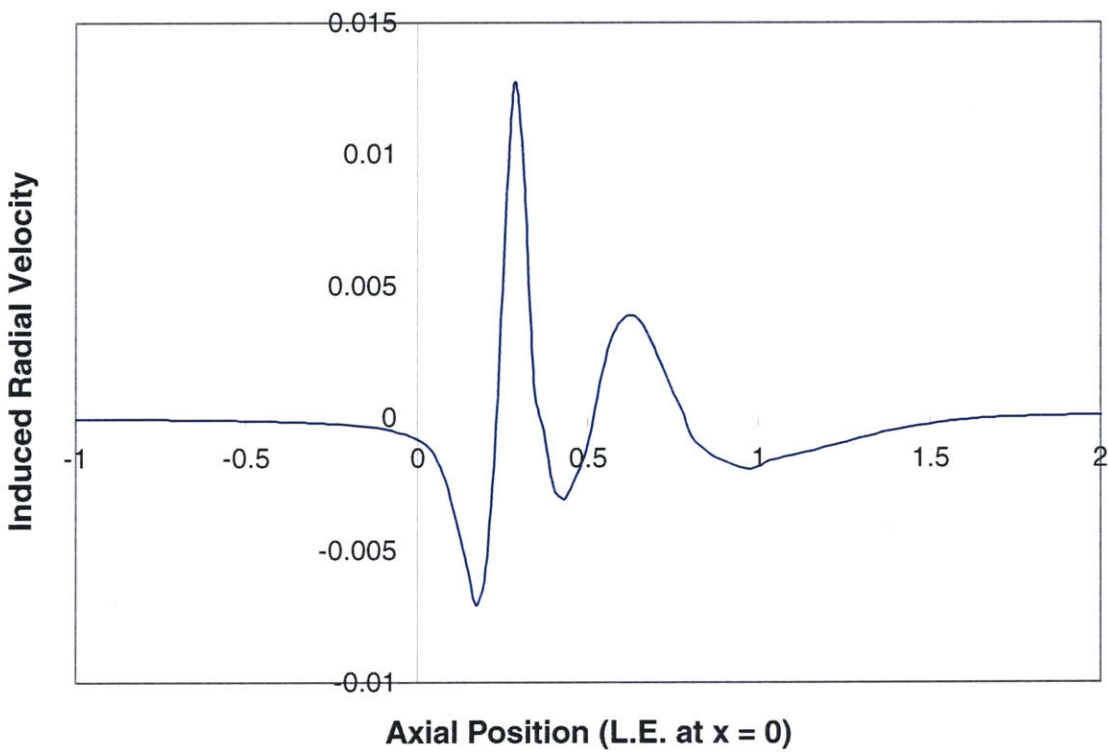
Fi
gure 5.9 Pitchwise-averaged radial velocity vs. axial location. Computed radial velocity for 100% groove at flow coefficient close to smoothwall design flow coefficient.

5.4 Causal Links

The results have shown that the radial transport term is important in increasing the streamwise momentum in the tip region, but a more detailed examination is necessary to determine causality and mechanisms that cause this change. The calculations show that change in radial transport of streamwise momentum is due to a repositioning of the tip clearance vortex with the groove, as shown in figure 5.10. This is why the change in radial velocity (refer to figure 5.6) exists in a region much larger than the extent of the groove. Figure 5.11 illustrates how a shift of the tip clearance vortex results in the double humped induced velocity profiles shown in figure 5.6.
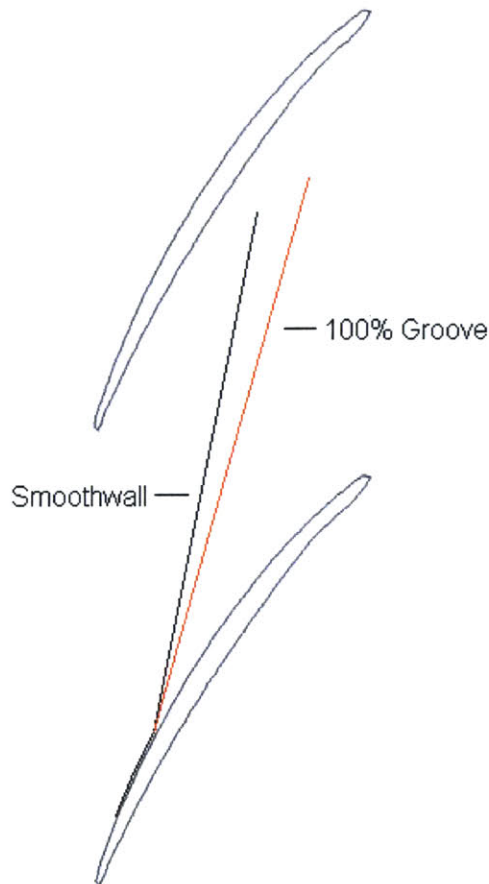
Figure 5.10 Change in vortex trajectory with use of the casing treatment (circumferential groove of depth equal to 100% of tip clearance gap).
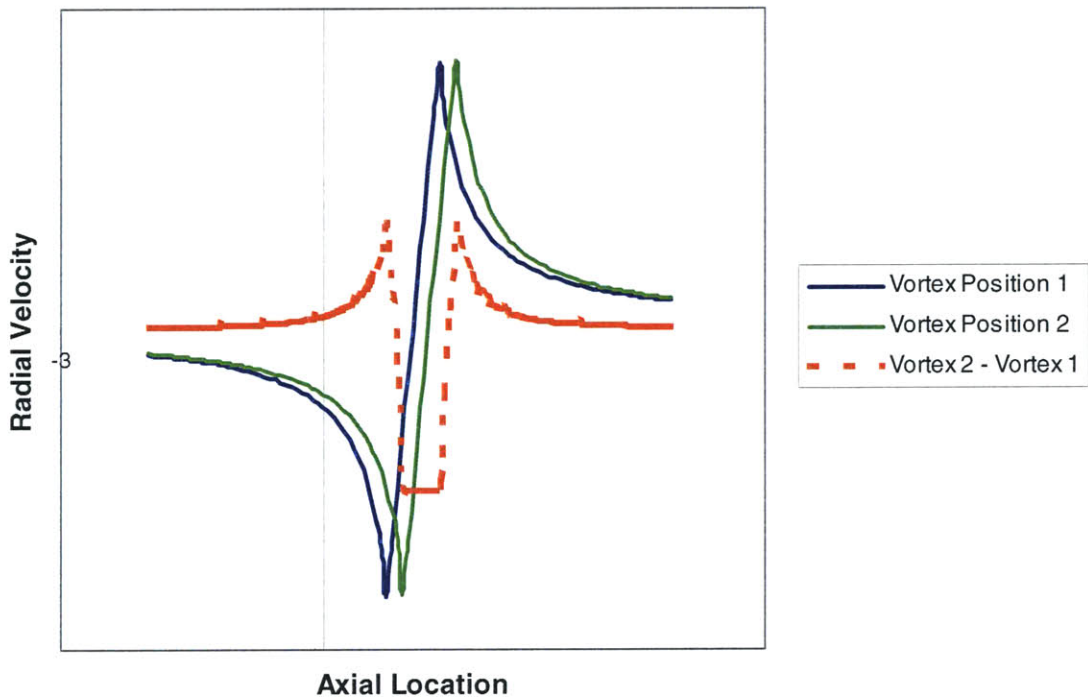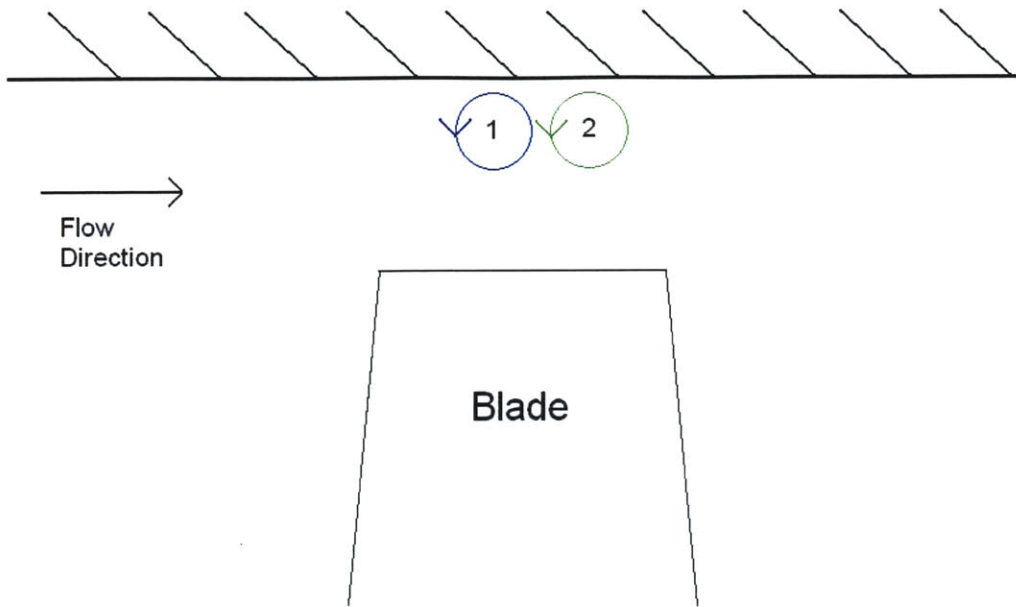
Figure 5.11 Illustration of change in radial velocity profile due to shift of clearance vortex. Two vortex positions are shown in (a). In (b), the velocity profiles that would result from these vortex positions are shown, in addition to the difference between the two profiles.

Since the vortex is now farther away from the leading edge, it is farther from the fluid

with the greatest streamwise velocity, and the effect of the of the vortex on the radial

transport is therefore reduced.

To change the position of the tip clearance vortex, there must first be some local

increase (relative to the smoothwall case) in the streamwise momentum. Circumferential

groove type casing treatment supply this increase through two routes:

- Radial exchange between the tip region and the grooves causes some reverse flow to be terminated by the walls of the groove, so there is a positive flux of momentum out of the grooves. This has been shown to be true using a simple integration of radial transport at the groove entrance ('Groove Flux' term in Table 3)
- Induced radial transport between the tip region and the main flow also increases streamwise momentum because outward radial velocity occurs closer to the leading edge, where streamwise velocity is greater. This local effect can be seen qualitatively in figure 5.12. It is a mechanism similar to that described in section 5.3, except on a smaller scale. This feature will be discussed further in sections 5.5 and 5.6.

The block diagram in figure 5.13 summarizes the events that lead to the increase

in streamwise momentum at the blade tip relative to the smoothwall. The two routes of

increased streamwise momentum result from the use of the casing treatment. As a result

of these local events, the clearance vortex is positioned further away from the leading

edge compared to the smoothwall case. This new vortex position results in a further

reduction of the debit of streamwise momentum from the tip region, which is a more

global effect.

2.61e-01
2.38e-01
2.15e-01
1.92e-01
1.69e-01
1.46e-01
1.23e-01
1.00e-01
7.69e-02
5.39e-02
3.09e-02
7.84e-03
-1.52e-02
-3.82e-02
-6.13e-02
-8.43e-02
-1.07e-01
-1.30e-01
-1.53e-01
-1.76e-01
-1.99e-01

beneficial local radial transport between tip flow and main flow
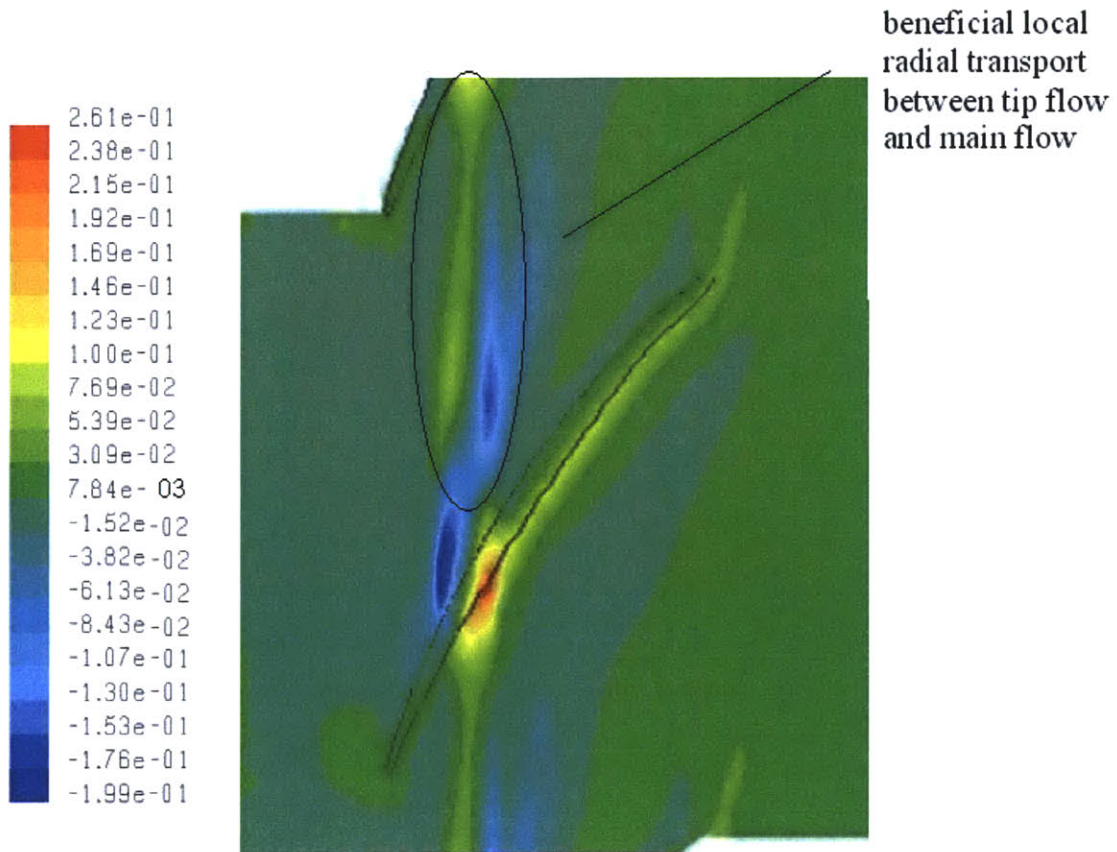
Figure 5.12 Qualitative view in the midgap of the local beneficial radial transport . Radial velocity contours are shown within the tip gap of the 100% groove case. The blue region is the inward radial velocity and marks the leading edge of the clearance vortex. The vortex is clearly pushed downstream by the flow field induced by the casing treatment.

```
┌─────────────────────────────────┐
│  radial velocity induced by casing │
│        treatment geometry         │
└─────────────────────────────────┘
         │                    │
         ▼                    ▼
┌──────────────────────┐  ┌──────────────────────────┐
│ some backflow flows into │  │ local radial transport bewteen │
│ casing groove and is stopped │  │   tip region and main flow   │
│       by the wall       │  └──────────────────────────┘
└──────────────────────┘                │
         │                              │
         ▼                              ▼
      ┌─────────────────────────────┐
      │      small increase in       │
      │     streamwise momentum      │
      └─────────────────────────────┘
                    │
                    ▼
┌─────────────────────────────────────┐
│ tip clearance vortex pushed back axially, │
│    further away from leading edge    │
└─────────────────────────────────────┘
                    │
                    ▼
┌──────────────────────────────────────────────────┐
│ increased distance from region of highest streamwise velocity │
│    reduces effect of vortex on the radial transport term     │
│         radial transport term greatly improved              │
└──────────────────────────────────────────────────┘
                    │
                    ▼
      ┌─────────────────────────────┐
      │  streamwise momentum in tip   │
      │    region improved further    │
      └─────────────────────────────┘
```

Figure 5.13 Block diagram showing role of casing treatment

5.5 Mechanism for Beneficial Local Radial Transport

The local radial transport mentioned in the previous section and illustrated in figure 5.12 is a result of the local groove-induced radial velocity, which results from the proximity of the tip clearance vortex to the groove. Figure 5.14 illustrates how this flow is produced when the tip clearance vortex is near the downstream edge of the circumferential groove. The flow field near the trailing edge of the groove is dominated by the influence of the clearance vortex, and has a large negative radial velocity. In order to satisfy continuity, there must be a positive radial velocity in the forward region of the groove. Figure 5.15 shows the computed relative velocity vectors (both smoothwall and 100% groove), confirming that this mechanism is responsible for the induced radial velocity. If the vortex is to far from the groove, the beneficial radial velocity will not be induced. Furthermore, if the groove is too shallow, boundary condition (no velocity perpendicular to the wall) on the groove wall will prevent the important changes in radial velocity.

(a)

Radial

Axial

Tip Clearance Vortex

(b)

Radial

Axial

Tip Clearance Vortex
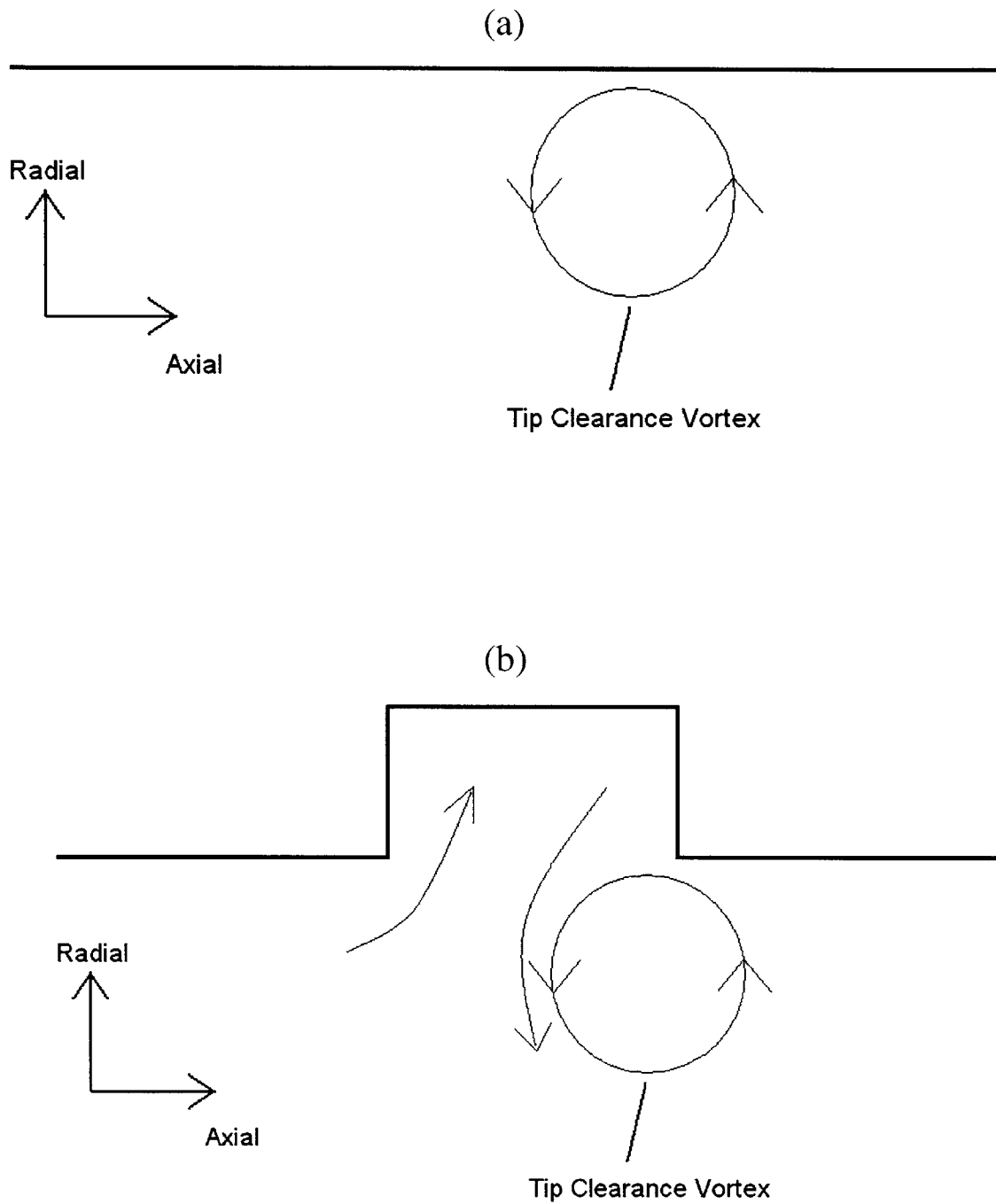
Figure 5.14 Mechanism for local radial transport improvement. Figure(a) shows the smoothwall case. Figure (b) shows the 100% groove case.
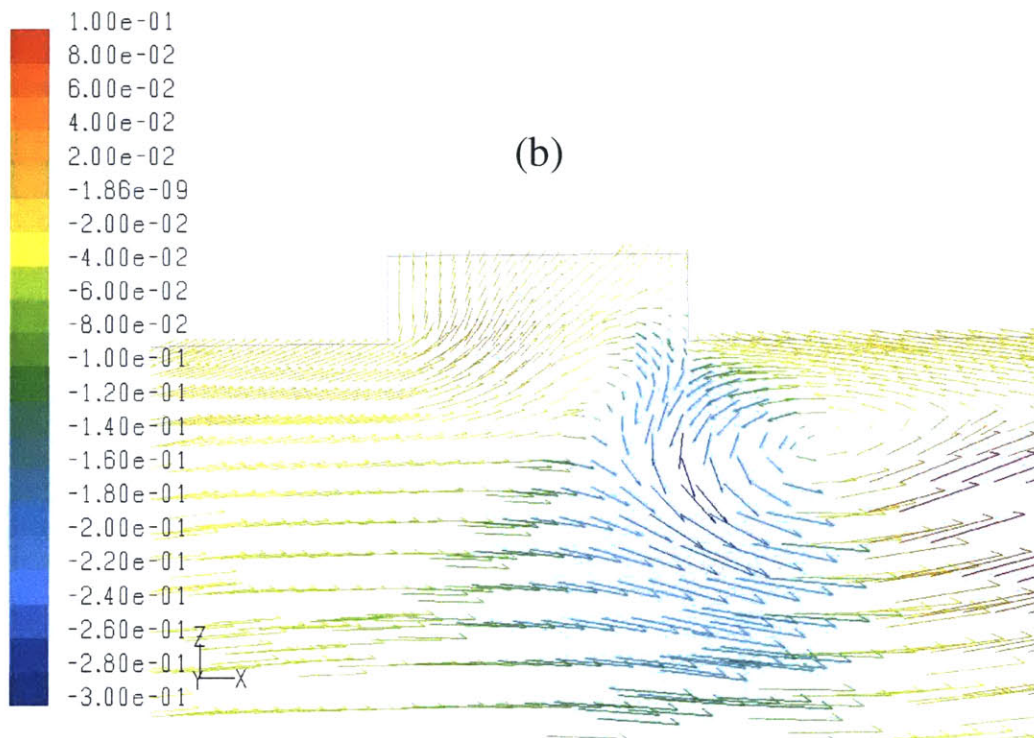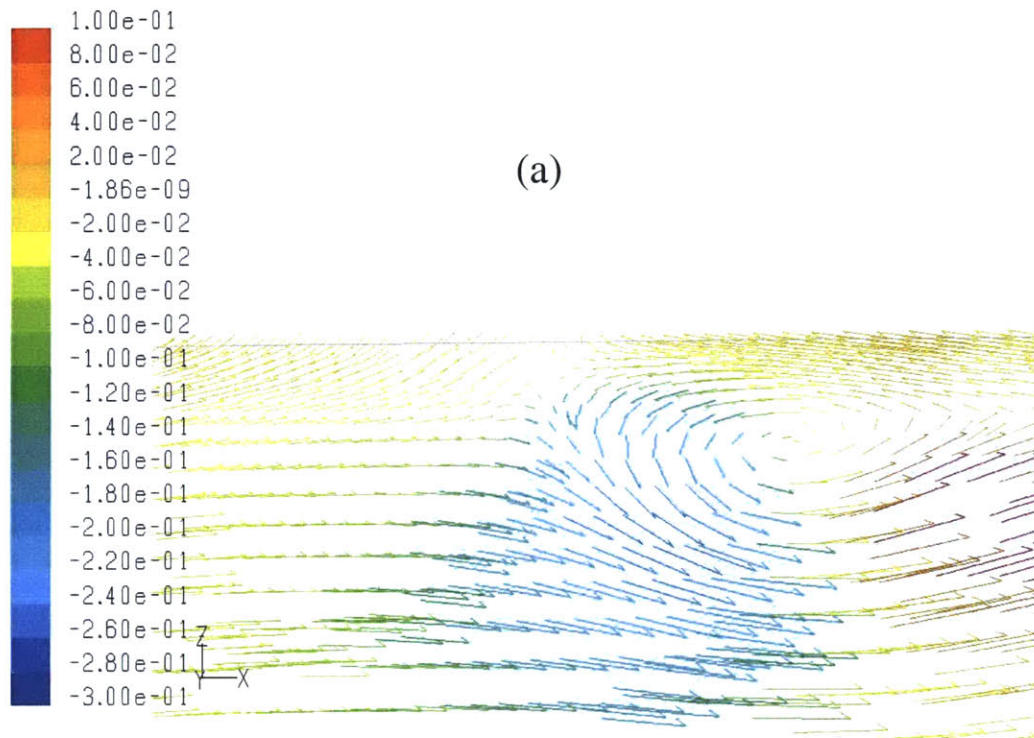
Figure 5.15 Relative velocity vectors at the mid-pitch. The vectors are colored by radial velocity, normalized by the blade tip speed. Both plots show the same axial extent, so direct comparisons can be made. Plot (a) shows the smoothwall case. Plot (b) shows the 100% groove case, illustrating the features sketched in figure 5.14.

To further assess some of the ideas regarding the interaction between the casing treatment and the clearance vortex, the circumferential groove casing geometry was altered. The groove was moved forward and centered at 5% axial chord, rather than at 25% chord position (Figure 5.16). Because the groove is now far ahead of the clearance vortex, this configuration was not effective and flow range was slightly worsened, as depicted in figure 5.17.

Groove ———

Blade ———
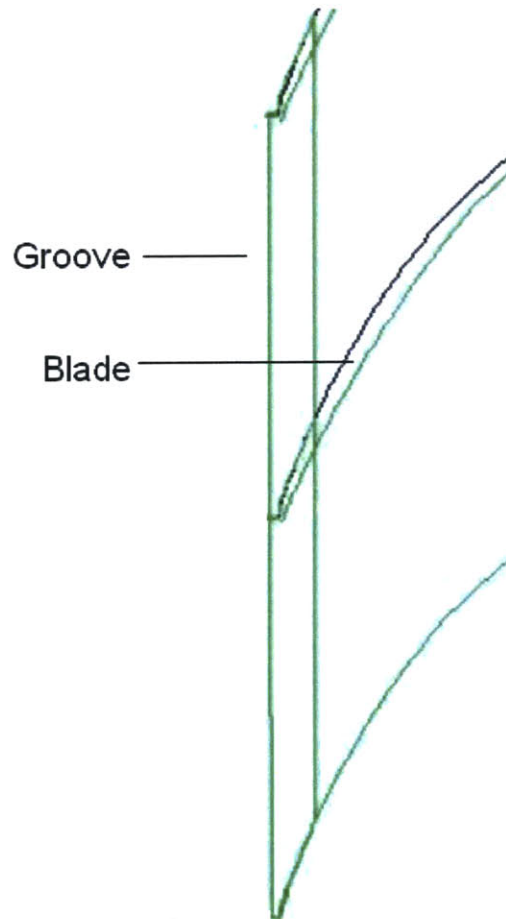
Figure 5.16 Groove forward position. This figure shows the groove axial position when centered at the 5% chord.
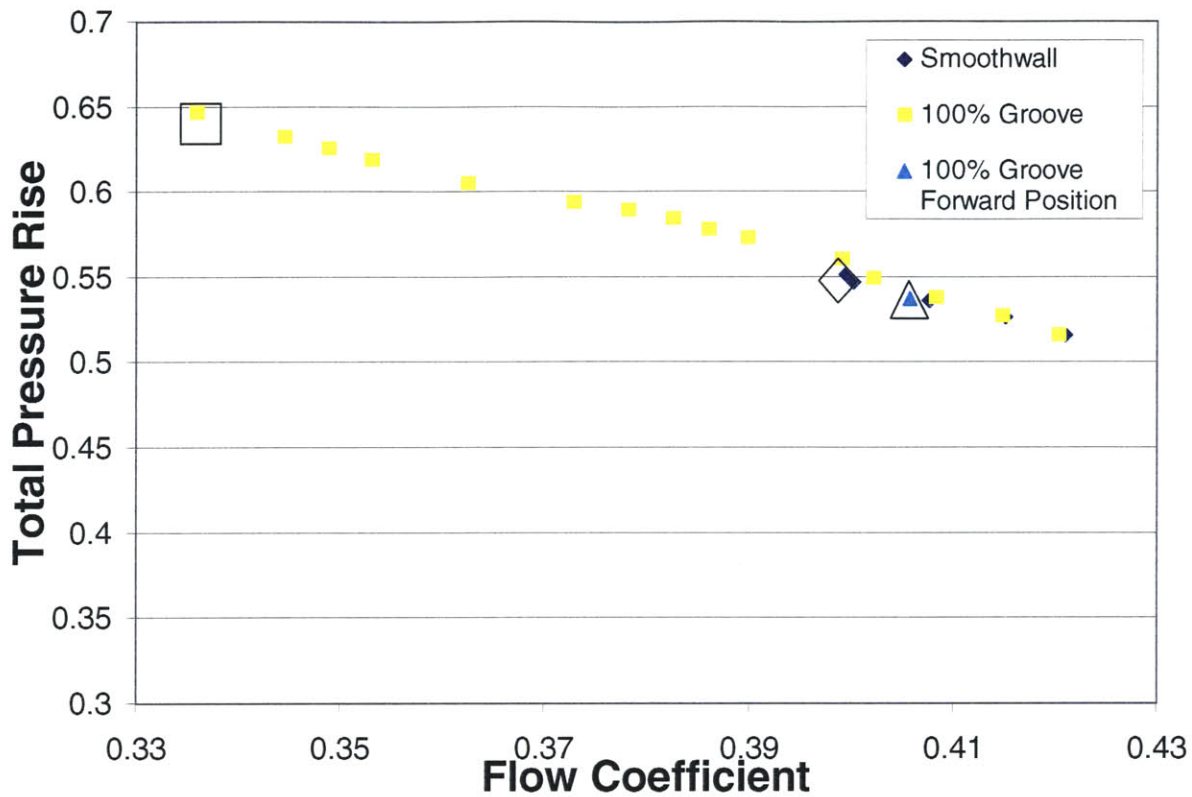
Figure 5.17 Total pressure rise coefficient vs. flow coefficient

The contours of radial velocity for two groove configurations are shown in Figures 5.18(a) and (b). Figure 5.18(a) confirms that the radial velocity associated with the beneficial local radial transport is not present when the groove is in the forward position centered at 5% chord. This is in contrast to the computed contour of radial velocity for the groove centered at 25% axial chord shown in figure 5.18(b), in which there is a region of large positive radial velocity at the mid-pitch of the groove leading edge. The vector plot in figure 5.19 confirms that the groove located at 5% chord is too far ahead of the vortex to induce the beneficial radial velocities.

(a) 5% chord position   (b) 25% chord position
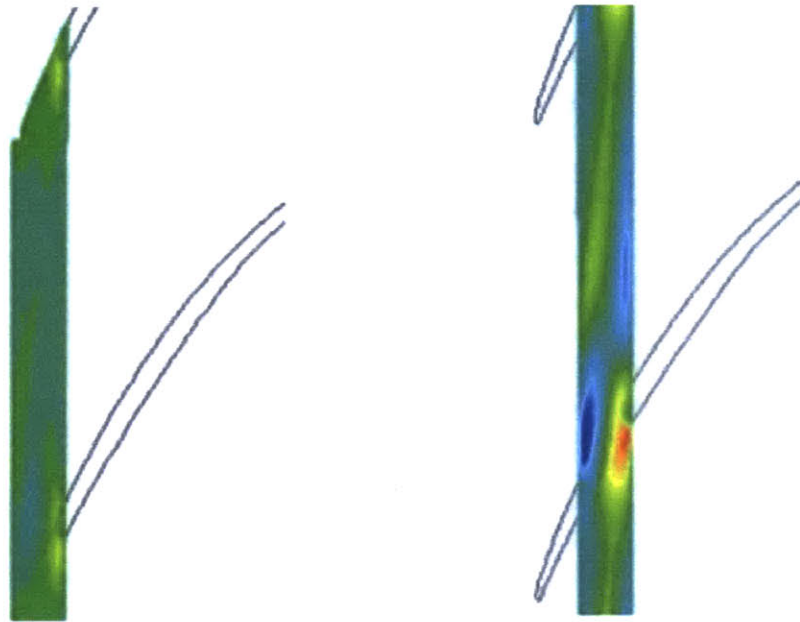
Figure 5.18 Radial velocity contours at the groove entrance, for both the original groove position and the forward groove position.
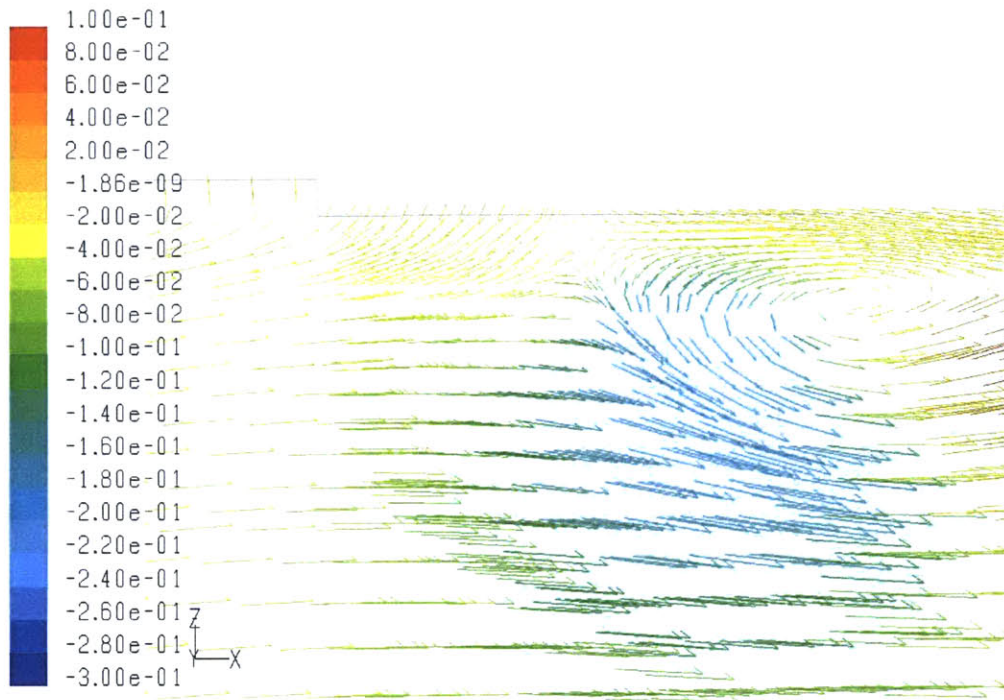
Figure 5.19Relative velocity vectors measured at the mid-pitch when the groove is centered on the 5% chord. This plot shows a greater axial extent than those in figure 5.15, which was necessary since the groove and vortex are much further apart. This further highlights the fact that the groove is too far ahead of the clearance vortex to induce the beneficial radial velocity.

5.6 Vortex Kinematics

It is possible that vortex kinematics may also be used to explain the shift in position of tip clearance vortex. In potential flow theory, an image vortex is used to satisfy the boundary condition that prevents normal velocity at the casing wall, as shown in figure 5.20. The flow field of the image vortex acts to force the tip clearance vortex upstream.
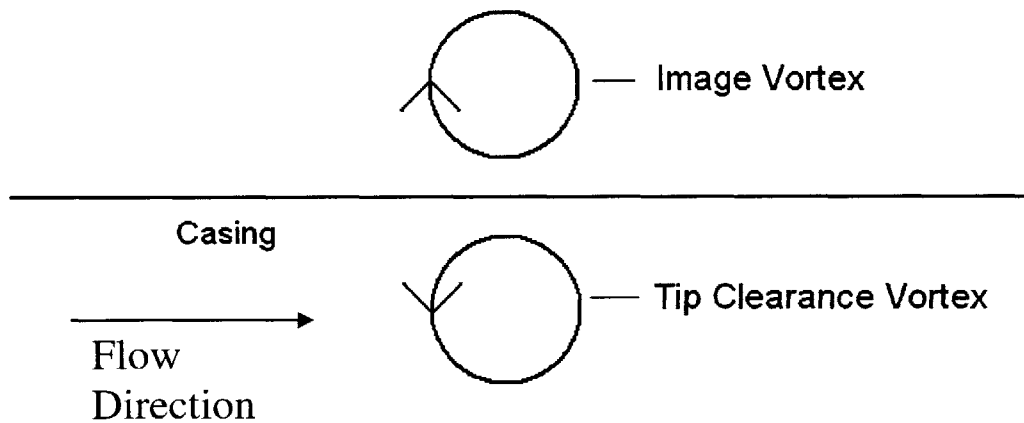
Figure 5.20 Image vortex system for the smoothwall case. The image vortex induces a flow field that tends to force the tip clearance vortex upstream.

The recession of the casing wall associated with the circumferential groove results in the image vortex being positioned further away from the tip clearance vortex, (see figure 5.21) and the upstream force on the clearance vortex is thus lessened. The image vortex system is more complicated than shown in figure 5.21, but the main features are captured by this simple model. If the clearance vortex is not in the vicinity of the groove, the image vortex will not be positioned further away from the clearance vortex when compared to the smoothwall case, and hence no improvement will be seen. This is

the same conclusion reached in the previous section, lending validity to this kinematics view of the circumferential groove action.
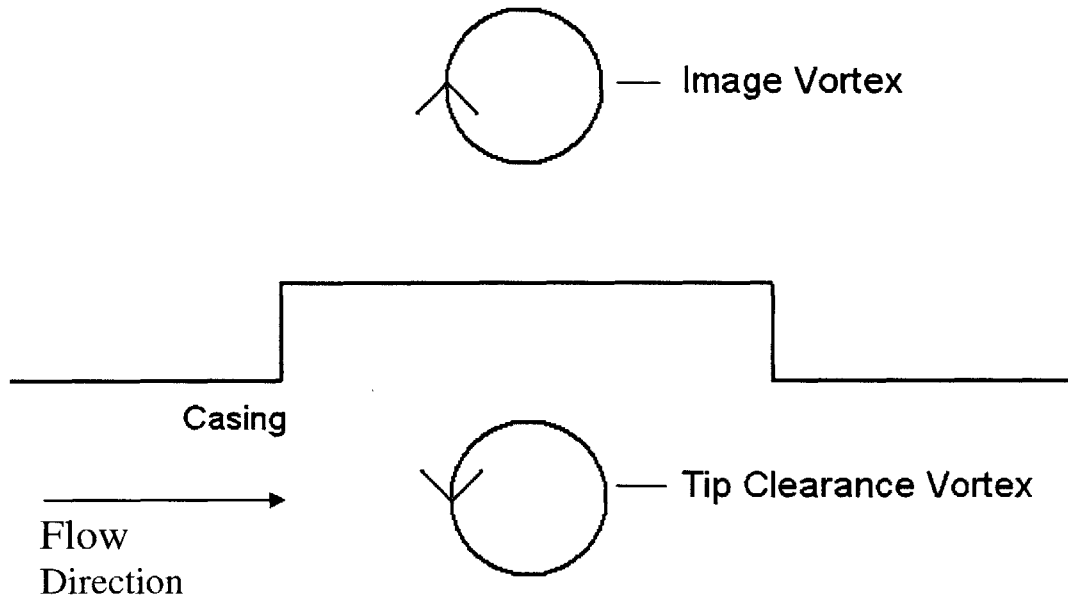
Figure 5.21 Image vortex system for the groove case. The image vortex is further away from the clearance vortex when compared to the smoothwall case.

5.7 General Guidelines for the Design of Groove Casing Treatment

Based upon the results presented in this research, the following design guidelines for circumferential groove casing treatments are suggested:

1) The depth of the groove does not have to be larger than the clearance gap in order to obtain a significant increase in flow range. In fact, nearly all of the flow range extension can be obtained with a groove depth that is half of the tip clearance gap. This is consistent with the work of Rabe and Hah [15] and Adamczyk and Shabbir[2].

2) Positioning the groove in the forward half of the blade passage is effective. It has been shown that the change in the radial transport of streamwise momentum is

dependent on the profile of streamwise velocity at the groove axial location. As most of the diffusion in streamwise velocity occurs only within the first half of the blade passage, the circumferential groove should be located in the first half of the blade passage. This consideration implies the groove should be located at the axial position where variation of streamwise velocity with axial position is the maximum (i.e. the slope of the curve in Fig. 5.5 is the most negative). However, in order for circumferential groove casing treatment to be beneficial and effective, the tip clearance vortex needs to be near the trailing edge of the circumferential groove.

3) One would need to focus on the leading edge region in designing new casing treatment. Any method of improving radial velocity in this region or lessening the impact on this region has the potential to improve the flow range.

4) We have not examined how the axial extent of the groove affects the flow range extension, but based upon the knowledge of how the casing treatment and tip clearance flow interact, some basic considerations can be outlined. The axial extent has to be large enough so that the radial velocity profile is appreciably changed. This sets the minimum axial extent needed to affect a flow range extension. If the extent becomes too large, however, the effective tip clearance gap would increase, thereby making the tip clearance vortex stronger and negating the beneficial effects of the casing treatment.

Chapter 6 Summary and Conclusions

1) Numerical experiments were performed to define the way in which tip clearance flow is altered by casing treatment to improve flow range.

2) This research corroborates previous research in that increased streamwise momentum at the blade tip is found to improve flow range in axial compressors. It extends these views, however, to show that a primary reason for the decrease in streamwise momentum within the tip region is that momentum is diverted inward by radial transport.

3) The radial velocity profile responsible for this transport is a result of the tip clearance vortex.

4) The effect of circumferential casing treatment is to alter the radial velocity profile in a manner that lessens the amount of streamwise momentum diverted out of the blade tip region.

5) To improve the radial transport term, the induced velocity should be towards the casing near the leading edge, and away from the casing near the trailing edge. Using circumferential groove type casing treatment, this is achieved by having the clearance vortex located towards the trailing edge.

6) Changes in the radial velocity very close to the circumferential groove provide the small, local, increase in momentum that affects the clearance vortex, as described in figure 5.14.

Chapter 7 Suggested Future Work

While suggested design guidelines for circumferential grooves and the intended effect of casing treatment have been described, the design process of casing treatment needs to be cast in a more quantitative basis.

Casing treatment should be assessed at different tip clearances. Since the routes to compressor instability (stall) can be dependent on tip clearance size, one should test different clearances to ensure that the findings are universally applicable to both spike and modal stall inceptions. The different stall inception processes are further elaborated in Appendix B.

This research used the geometry of a low-speed machine. Whether the findings described in this research apply to the transonic regime should be addressed. It is the author's opinion that while the shock structure will complicate the tip flow structure, the findings should be applicable to a high-speed compressor.

References

[1] Adamczyk, J. J., Celestina, M. L., and Greitzer, E. M., 1993, "The Role of Tip Clearance in High-Speed Fan Stall,", ASME Journal of Turbomachinery, Transactions of the ASME, Vol. 115, January 1993.

[2] Adamczyk, J.J. and Shabbir, A., "Flow Mechanism for Stall Margin Improvement due to Circumferential Casing Grooves on Axial Compressors", ASME Turbo Expo 2004, paper GT2004-53903.

[3] Camp, T.R., and Day, I.J., "A Study of Spike and Modal Stall Phenomena in a Low-Speed Axial Compressor", ASME Journal of Turbomachinery 97-GT-526, June 1997.

[4] Chen, G. T., Greitzer, E.M., Tan, C.S. and Marble, F.E.,"Similarity Analysis of Compressor Tip Clearance Flow Structure", ASME Journal of Turbomachinery, Vol 113, pp 260-271, April 1991.

[5] Crook, A.J., Greitzer, E.M., Tan, C.S., and Adamczyk, J.J., 1993, "Numerical Simulation of Compressor Endwall and Casing Treatment Flow Phenomena", ASME J. Turbomachinery, Vol. 115, No. 3, 501-512.

[6] Cumpsty, N.A.,Compressor Aerodynamics, Longman Group UK Ltd., London, England, 1989.

[7] Gong, Y., Tan, C.S., Gordon, K.A., and Greitzer, E.M., "A Computational Model for Short Wavelength Stall Inception and Development in Multi-Stage Compressors", ASME Journal of Turbomachinery, 98-GT-476, June 1998.

[8] Greitzer, E.M., Nikkanen, J.P., Haddad, D.E., Mazzawy, R.S., Joslyn, H.D., "A Fundamental Criterion for the Application of Rotor Casing Treatment", Journal of Fluids Engineering, Vol. 101, June 1979.

[9] Greitzer, E.M., Tan, C.S., Graf, M.B., Internal Flow, Concepts and Applications, Cambridge University Press, 2005.

[10] Hill, P.P, and Peterson, C.R., "Mechanics and Thermodynamics of Propulsion", Addison-Wesley Publishing, 1992.

[11] Lee, N.K.W. and Greitzer, E.M., "Effects of Endwall Suction and Blowing on Axial Compressor Stability Enhancement", ASME Journal of Turbomachinery, Vol. 112, pp.133-144, January 1990.

[12] Kerrebrock, J.L. Aircraft Engines and Gas Turbines, 2nd Edition. MIT Press, 1992.

[13] Khalid, S.A., Khalsa, A.S., Waitz, I.A., Tan, C.S., Greitzer, E.M., Cumpsty, N.A., Adamczyk, J.J. and Marble, F.E., "Endwall Blockage in Axial Compressors", <u>ASME Journal of Turbomachinery</u>, Vol. 121, pp.499-509, July 1999.

[14] Koch, C. C., "Stalling Pressure Rise Capability of Axial Flow Compressor Stages," ASME J. Eng. Power, 103, pp. 645–656, 1981.

[15] Rabe, D.C., Hah, C.,2002, "Application of Casing Circumferential Grooves for Improved Stall Margin in a Transonic Axial Compressor", ASME Turbo Expo 2002, paper GT-2002-30641.

[16] Seitz, P.A. "Casing Treatment for Axial Flow Compressors", Cambridge University Ph.D. dissertation, April 1999.

[17] Storer, J.A. and Cumpsty, N.A., "Tip Leakage Flow in Axial Compressors", <u>ASME Journal of Turbomachinery</u>, Vol. 113, pp.252-259, April 1991.

[18] Thompson, D.W., and King, P.I., Hah, C., and Rabe, D.C., "Experimental and Computational Investigation of Stepped Tip Gap Effects on the Flowfield of a Transonic Axial-Flow Compressor Rotor", ASME Journal of Turbomachinery, 98-GT-90, June 1998.

[19] Vo, H. D., "Role of Tip Clearance Flow on Axial Compressor Stability", Massachusetts Institute of Technology, Ph.D. Thesis, September 2001.

Appendix A User-Defined Function

The custom code that communicates with Fluent to determine the Body Force

vectors is shown here. The force per volume distribution (as a function of position and

relative velocity field) is the output of the code. The radial extent in which the algorithm

is to be applied first needs to be specified within Fluent.

```
#include "udf.h"

DEFINE_ADJUST(v_adjust,domain)
{

int id = 1;
cell_t cell;
Thread *thread = Lookup_Thread(domain,1);

}


DEFINE_SOURCE(cell_x3_source, cell, thread, dS, eqn)
{
  real x[ND_ND];
  real Fx;
  real Fy;
  real vx;
  real vy;
  real theta;
  real source1;
  real x1,y1,z1,r_local;
  real vmag, Fmag;

//Variables representing the position of the cells
  C_CENTROID(x,cell,thread);
  x1 = x[0];
  y1 = x[1];
  z1 = x[2];

//Find the radial position of the cells
  r_local = sqrt(pow(y1,2)+pow(z1,2));


//Find the relative axial and circumferential velocities
  vx = C_U(cell,thread);
  vy = C_V(cell,thread) + 223*r_local;

//Calculate the total relative velocity
  vmag = sqrt(pow(vx,2)+pow(vy,2));
//Scale the body force proportionally with the relative velocity
```

```
//7163 is the factor for Casing Force(high); 2000 for Casing Force(Low)
  Fmag = 7163*vmag;
//The radial extent of the force can easily be specified in Fluent, but
//it is easier to express the axial extent here.  Only within the axial
//extent of the blade tip will the body force be applied

  if(x1 < -0.02313)
  Fmag = 0;

  if(x1 > 0.02938)
  Fmag = 0;

//Calculate the relative velocity angle
  theta = atan(vy/vx);

//Calulate the axial component of the Body Force
  Fx = Fmag*sin(theta);

//The x-component of the body force should always be pointed downstream
  if(Fx < 0)
  Fx = -Fx;

  source1 = Fx;

//C_UDMI(cell,thread,0) = source1;

  dS[eqn] = 0;

  return source1;

}

//The determination of the tangential component of the body force is
//done in the same manner as the axial component.  Much of the code
//could be combined, but it worked as shown, so it was left in this
//form
DEFINE_SOURCE(cell_y3_source, cell, thread, dS, eqn)
{

  real x[ND_ND];
  real Fx;
  real Fy;
  real vx;
  real vy;
  real theta;
  real source2;
  real x1,y1,z1,r_local;
  real vmag, Fmag;

  C_CENTROID(x,cell,thread);
  x1 = x[0];
  y1 = x[1];
  z1 = x[2];

  r_local = sqrt(pow(y1,2)+pow(z1,2));

  vx = C_U(cell,thread);
```

```
  vy = C_V(cell,thread) + 223*r_local;

  vmag = sqrt(pow(vx,2)+pow(vy,2));
  Fmag = 7163*vmag;

  if(x1 < -0.02313)
  Fmag = 0;

  if(x1 > 0.02938)
  Fmag = 0;

  theta = atan(vy/vx);

  Fy = -Fmag*cos(theta);

//The axial component is made to point downstream, and the tangential
//component direction is fixed by this decision.
  if(vx*vy < 0. && Fy < 0.)
  Fy = -Fy;

  if(vx*vy > 0. && Fy > 0.)
  Fy = -Fy;

  source2 = Fy;

  dS[eqn] = 0;

  return source2;

}
```

Appendix B Method of Stall Inception

There are two stall inception methods: modal stall and spike stall [Day and Camp, 3]. Modal stall occur when a long-wavelength disturbance (one the order or of the annulus distance) grows slowly into fully developed stall cells. Spike stall, on the other hand, occurs when a short-wavelength (2-3 blade passages) triggers a stall within a few rotor revolutions [Day and Camp, 3]. Vo [16] outlined the flow field characteristics that accompany spike stall. If the last converged solution does not exhibit the limit of stable flow according to the spike stall criteria, then it is modal stall that is responsible for the inception.

Figure A.1, from Vo [16] compares the flow field characteristic immediately preceding the different types of stall. When spike stall is the limiter, the high entropy gradient at the blade tip is aligned with the blade passage entrance. When modal stall is the inception route, the interface remains well within the blade passage. Vo achieved the two different types of characteristics in the same blade geometry by varying the tip clearance gap. From the entropy contours of the present calculation (shown in Fig. A.2), one can see that the interface is located well within the blade passage, suggesting that this geometry has a flow range limited by modal stall. Vo also found that an E^3 Rotor with 3% chord tip clearance gap, which is the geometry used in the present research, is characterized by modal stall inception.

This work focuses on the physics behind the beneficial effects of casing treatments, so the inception route may not be of primary importance. We note that the mechanisms here were for a compressor with modal type of stall, and some features of casing treatment may change if the type of stall changes.
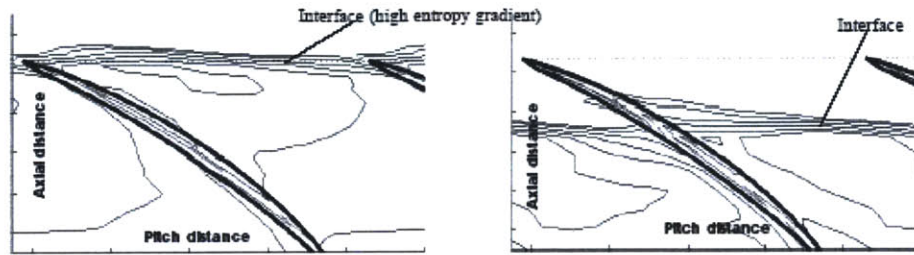
Figure B.1 Comparison of flow fields at blade tip immediately preceding spike and modal stalls
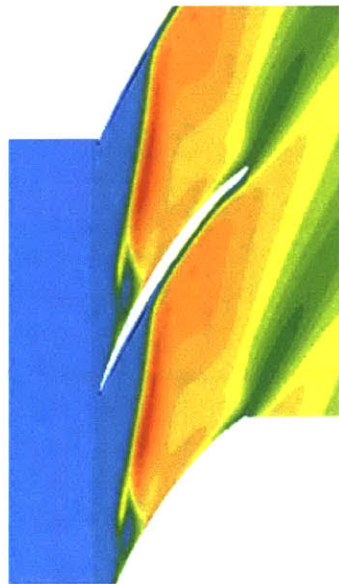

Figure B.2 Entropy contours at 100% span. The high-entropy interface is well within the blade passage.

When the relative flow angle at the leading edge in a spike-limited compressor reaches a critical angle, stall occurs. As the compressor is pushed further towards stall, the incidence increases until this limit is reached (assuming modal stall does not occur first). Table 4, however, shows that because the casing treatment reduces the incidence angle at a given flow coefficient, it is likely the treatment is also effective if spike disturbance is the stall inception method

Table 4 Flow angle at blade tip leading edge at the smoothwall stall flow coefficient. Note that the presence of the casing treatment reduces the flow angle at the blade tip leading edge.

Geometry	Relative Flow Angle
Smoothwall	75.6 degrees
5% Groove	74.4
10% Groove	73.5
100% Groove	73.8

Appendix C Sensitivity to Turbulence Model

In the current research, one of the most surprising results was the ability of the 5% groove to affect a substantial change in the flow range over the smoothwall case. This prompted a study to ensure that the results were indicative of changes in the flow field, and not due to poor modeling by the CFD calculation.

First the grid was examined to determine if the cell density was high enough. Standard wall functions are used on every solid surface in order to reduce the number of cells needed to run the calculation. Wall functions estimate the effect of the viscous boundary layer without actually fully resolving the boundary layer. For wall functions to operate correctly, the cell size adjacent to wall in question must be a particular size. The distance of importance is called the y+ value, described by the equation,

$$y^+ = \frac{\rho u_\tau y}{\mu} \tag{C.1}$$

The y+ values present in theses calculations are between 30 and 80, which is within the acceptable range.

After confirming the adequacy of cell density, the turbulence model was tested. The wall functions were changed from standard to non-equilibrium wall functions. As another test, the entire turbulence model was changed from standard k-epsilon to Spalart-Allmaras. Using these different tools of turbulence models, a few points were calculated for both the smoothwall and the 5% Groove. The results from these calculations are shown in Fig. C.1 and Fig C.2. Although the absolute values of the pressure rise, stalling flow coefficients, and efficiencies change as a result of the different turbulence models, the relative changes are comparable. These interrogations of the grid and alterations of

the turbulence models show that the conclusions are relatively independent to turbulence model.
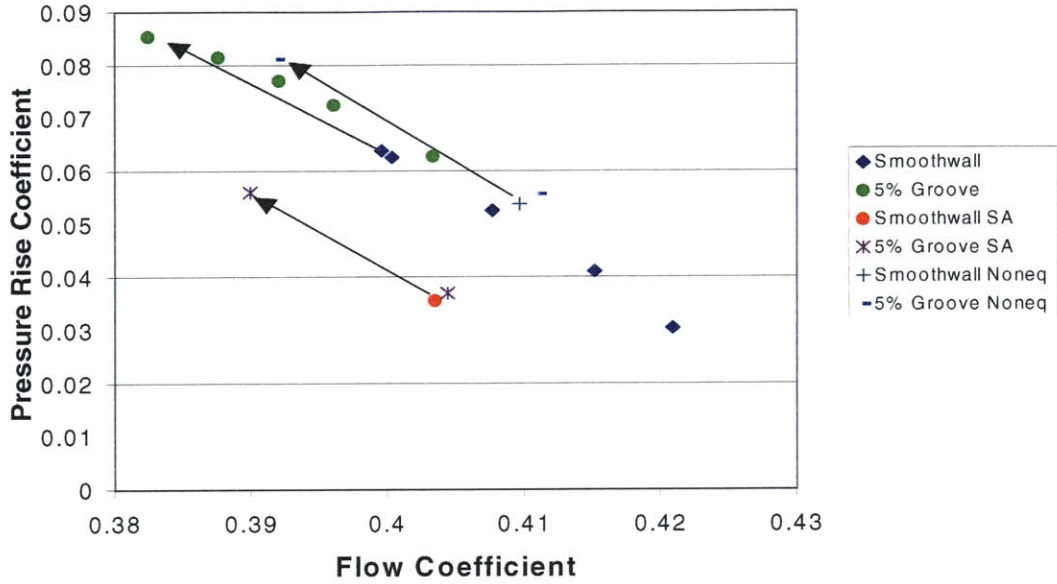

Figure C.1 Pressure rise coefficient vs. flow coefficient. Results using Spalart-Allmaras and non-equilibrium wall functions are shown. The arrows show the change in stall point between the smoothwall and the 5% groove. The change is similar for all three turbulence model setups.
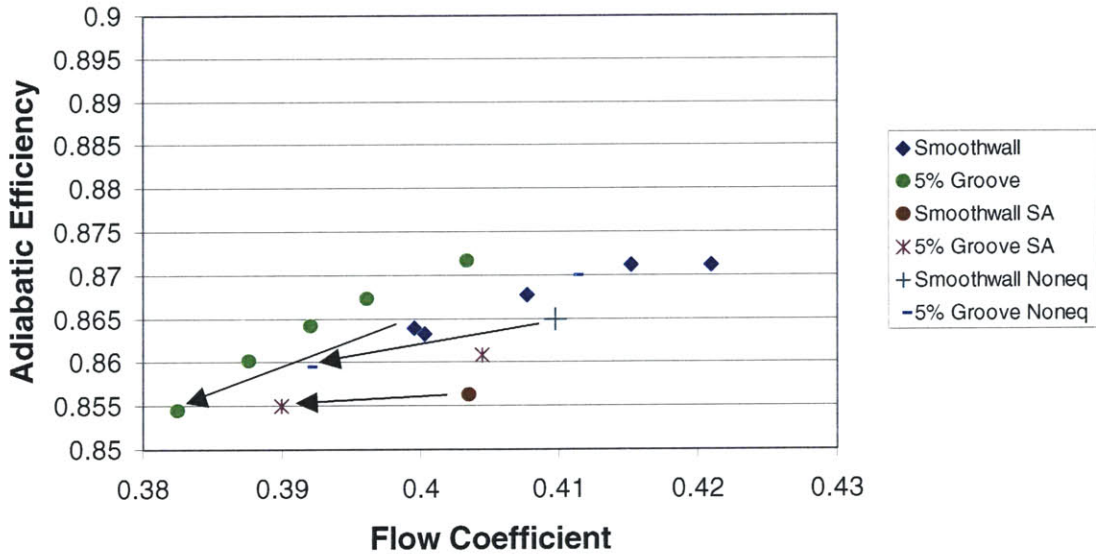

Figure C.2 Adiabatic efficiency vs. flow coefficient. The arrows show the change in stall point using the 5% groove. Once again, the change is similar regardless of the turbulence model.